MULTISPECTRAL IMAGER

USING BAND PASS OPTICAL FILTERS AND

IMAGE ILLUMINATION CORRECTION

by

Akshay Chavan, BE.

A Thesis

In

ELECTRICAL AND COMPUTER ENGINEERING

Submitted to the Graduate Faculty
of Texas Tech University in
Partial Fulfillment of
the Requirements for
the Degree of

MASTER OF SCIENCE
IN
ELECTRICAL ENGINEERING

Approved

Dr. Brian Nutter
Chair

Dr. Sunanda Mitra

Peggy Gordon Miller
Dean of the Graduate School

August, 2011

ACKNOWLEDGMENTS

TABLE OF CONTENTS

ABSTRACT

Commercially available multispectral or hyperspectral imaging systems are designed to capture images, at predefined wavelength intervals. Various mechanisms are implemented for changing the wavelength intervals of light used for capturing spectral images, and any variations in these frequency intervals require major alterations. Dispersion of light is carried out either by diffraction gratings or by electronically tunable filters. Apparatus with diffraction grating are inexpensive but have slow response time. Electronically tunable filters have quick response time but make the apparatus expensive.

Imaging systems where optical filters are mounted on a rotating disc to capture hyperspectral images have a predefined utility because there is no means to select or adjust the filters that are placed on the disc for a given experiment.

The proposed approach includes the use of step up rings to attach the optical filters with threaded c-mount attachments to the holes in a metal disc. The use of step up rings to mount the optical filters provides a way to replace filters effortlessly. As a result, the system has additional research functionality to be used as a test structure to evaluate the performance of the filters, based on their response and the selection of central frequency according to the requirements of an experiment.

The precision processing of light required while using diffraction gratings or tunable filters can be avoided by the use of optical filters. The assembly with optical filters does not require precise control on the disc, to position the filters in front of the camera.

The proposed assembly also provides a prototype that can be improved to accelerate the process of image acquisition, which will make the apparatus faster than the one with diffraction grating and less expensive than the one with tunable filters.

LIST OF TABLES

LIST OF FIGURES

CHAPTER I

INTRODUCTION

Approximately 170 years ago, compounds such as silver chloride and silver nitrate were used for the first time to develop images. These materials responded and reacted differently to light than other substances. These substances darken on exposure to light, and we capture images and classify the materials according to the reaction to light exposure.

Color images are basically multispectral images consisting of images from red (around 575 nm), green (around 535 nm) and blue (around 445 nm) spectral bands captured separately [1]. Multispectral imaging and hyperspectral imaging are based on the same principle of capturing multiple images of a scene or object using light from different parts of the spectrum. Multispectral imaging consists of taking images with discrete wavelength bands (around 20), which are narrower than the ones used for generation of a RGB image. Similarly, hyperspectral imaging captures images with very narrow spectral bands (around 100) on a contiguous spectral range that produces spectra for all the pixels in the image [2]. The prefix "hyper" in hyperspectral refers to "over" or "excess" of spectral bands used to form a stack of images over the spectrum of light. Hyperspectral images are captured from many spectral bands over the light spectrum range from visible to infrared.

Hyperspectral images are used for quantitative analysis using the spectral characteristics of a material according to its reflectance properties, which are analyzed by the intensity response in the spectral images that are captured. This method requires a spectral library to be used as reference for the spectral characteristics of the particular material or substance over the frequency range. If the material exists in the image, it can be detected by matching the intensity response over the frequency range to the available reference response.

Hyperspectral imaging is traditionally used in remote sensing applications as well as target detection, material mapping, material identification and mapping details of surface properties [3].

Hyperspectral imaging for target detection is normally used in defense operations, for example to detect camouflaged military vehicles under a partial vegetation canopy. It is also used to detect vegetation species in a particular area and to detect oil seeps or oil impacted soils. Material mapping is also performed when the materials such as vegetation present in the scene are known in advance. It has also been used to map heavy metals and other toxic wastes within mine tailings in active and historic mining districts. Material identification tests the intensity response of the pixels to determine whether they match some known material responses. Hyperspectral imagery has also been used to study details of surface properties that are difficult to detect using other types of imagery, such as soil moisture, organic content, and salinity. The application of detecting surface properties along with the material mapping property will be proposed for a medical application in this project. Detecting hemoglobin and melanin content and toxic materials that could have formed on wounds undergoing the healing process is a means to superficially analyze the health of the skin. This could also be called tracking the wound healing process.

Matched filtering is a technique to map only the user required targets and not all the spectra available from the hyperspectral cube. Matched filtering was originally developed to identify targets in the scene that are relatively rare [4].

Hyperspectral sensors or cameras that are modified to capture hyperspectral images and collect spectral information for aerial and laboratory applications are discussed in section 2 of this chapter.

Hyperspectral imaging has found many applications other than remote sensing, including face detection, determination of oxy-hemoglobin content in skin and blood,

studying diabetic ulcers and wound analysis, pharmaceutical manufacturing, microscopy, life sciences and biotechnology, forensics, food safety and quality and many more.

1.1. Objectives

Multispectral and hyperspectral imaging systems that are commercially available are manufactured according to some predefined filter sets that are useful for specific applications. Manipulation of light is required by using color wheels, diffraction gratings, or electronically tunable filters. Apparatus with diffraction gratings have slower response time because the imaging system must be physically moved across the area to be imaged. The electronically tunable filters make the system more expensive but faster.

Imaging systems with optical filters mounted on a rotating disc to capture hyperspectral images are available. They are designed to perform a particular procedure, i.e. to capture images at predefined frequency intervals with no innate provision to selecting a frequency or the width of the light spectrum to form an image.

The main objective of this thesis project is to build a multispectral imager that will facilitate capture of images at different frequency intervals of light for medical applications. The system will have provision for replacing the optical filters because the optical filters will be mounted on step up rings glued into holes in the disc. An easy method of replacing filters will facilitate the response evaluation according to the requirement of an experiment, making the apparatus suitable as a test structure for research purposes.

The assembly will be a prototype for large scale manufacturing of an inexpensive image acquisition system for hyperspectral imaging with the functionality

of detachable filters. This apparatus will have faster response than the one using diffraction gratings and be less expensive than the one with tunable filters.

1.2. Previous work

Many different methods have been developed in which a camera can be modified to capture images at different predefined spectral values. Two basic techniques have been developed to modify a camera to capture hyperspectral images. In one the techniques, a narrow band of light dispersed using diffraction grating or bandpass filter is used to develop images. The second technique modifies the light source to emit only a particular band of light to illuminate the subject of interest and the light reflected from the subject is allowed to reach the camera's sensor to form an image.

A basic principle regarding the diffraction grating apparatus is to implement the scattering of light with a prism and then use small contiguous bands from this spectrum of light to form a stack of images. Figure 1 shows a schematic representation of white light being scattered by a prism.
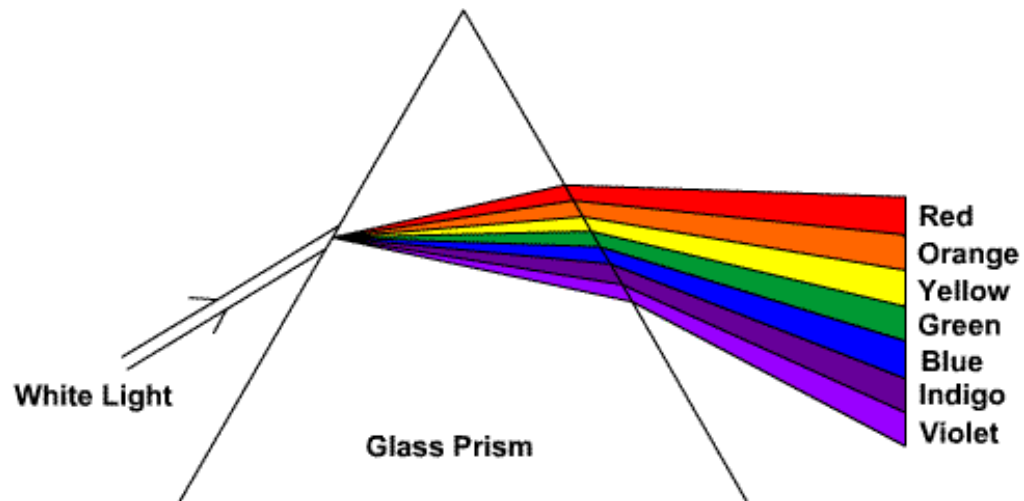
Figure 1. Schematic representation of scattering of white light

The most widely used application of hyperspectral imaging is aerial remote sensing, where the principle of dispersion of light is implemented using diffraction gratings as an optical element to separate incident light into its constituent wavelengths.

A diffraction grating is a pattern of equally spaced parallel silts, wedges or grooves of reflecting or transmitting elements separated to emit narrow bands of light. Two different types of gratings have been developed: reflection grating, made up of a grating mounted on a reflecting substrate and transmission grating, where the grating is mounted on a transparent substrate [5]. The spectral range to select depends on the starting wavelength of the grating and the number of grating lines/mm.
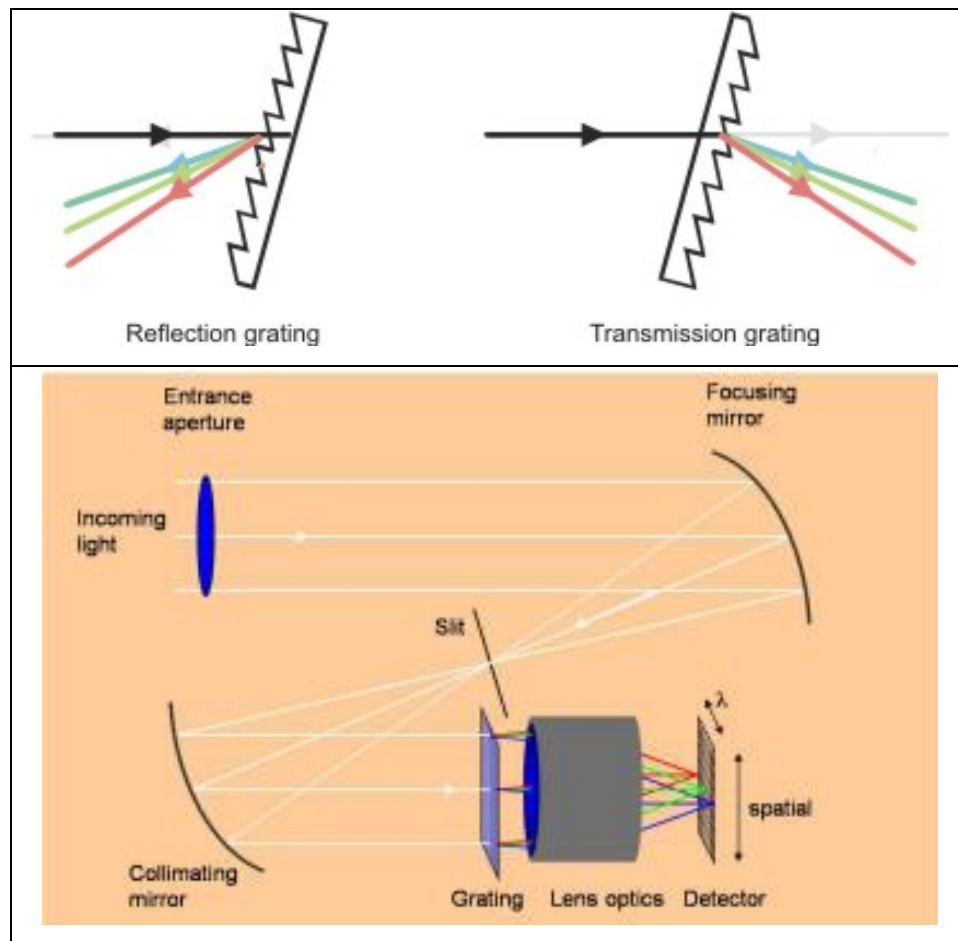
Figure 2. Schematic of reflection grating and its usage in spectrometry

5

The basic principle of the grating can be explained with Figure 2. The incoming light is collimated through a slit using a converging lens, and this light is then passed through the transmission gratings, which split the light into spectral bands that are then projected onto detectors aligned to measure the image spectrum for that particular pixel. This process is carried out over the entire region of the subject of interest, a small portion at a time, which represents a pixel in the image. To get a continuous image of the ground, the camera assembly in an aircraft or satellite is made to move in a 'pushbroom' mode or 'whiskbroom' mode depending on whether an array of detectors is used or only a single detector is used for each frequency band.

Figure 3 shows the two modes of movements required according to the type of detectors used.
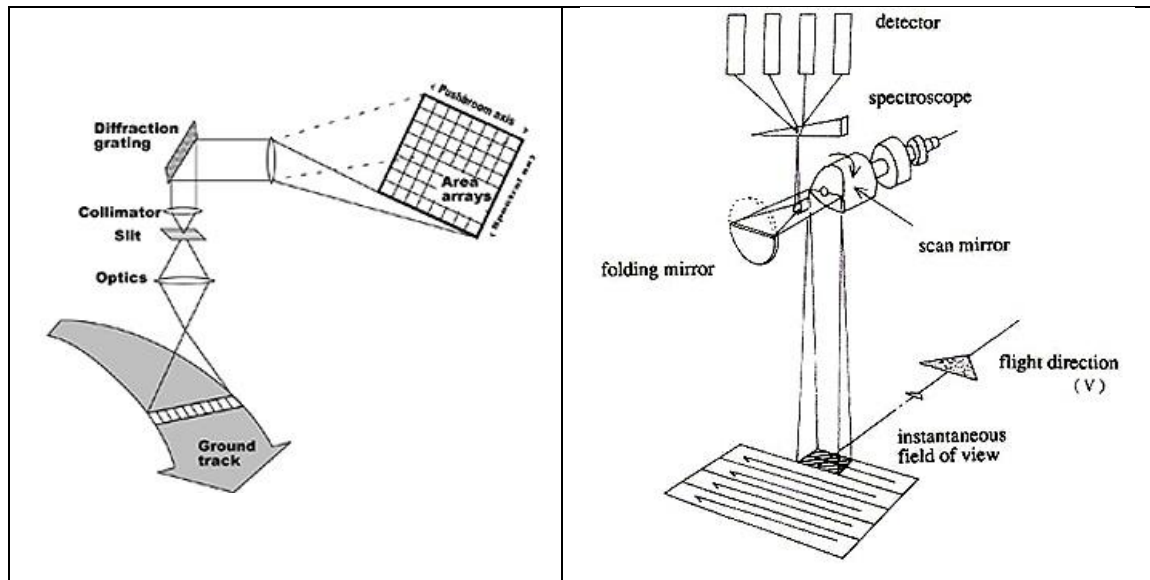
Figure 3. Pushbroom movement and whiskbroom movement [6]

In the pushbroom mode, the array of detectors forms the first dimension, the "pushbroom" action forms the second dimension and the third dimension is the spectral dimension formed by the diffraction grating.

A number of modified implementations are available from the companies providing cameras for hyperspectral imaging. HySpex is one of the commercial manufacturers of hyperspectral cameras. After collimating the light entering through a narrow slit, the transmission grating separates the light into different wavelength bands, and the light is then focused onto a detector array. The net effect of the optics is that for each pixel interval along the line defined by the slit, a corresponding spectrum is projected on a column of detectors on the array. "By scanning over the scene, the HySpex camera collects slices from adjacent lines, forming a hyperspectral image or 'cube', with two spatial dimensions and one spectral dimension. [7]" This technique of imaging can also be applied to scan stationary images.

Chenghai Yang, et al., implemented a system based on CCD cameras that can be applied for airborne remote sensing applications as well as stationary laboratory applications [8]. The airborne configuration consisted of a digital camera, an imaging spectrograph and a front lens, while the only addition to the stationary configuration was a focal plane scanner attached between the imaging spectrograph via an adapter and the front lens via a C-mount. A CMA-12CC linear actuator from Newport Corporation that provides a wide range of speed with precision motion was used to drive the focal plane scanner either manually by an operator or automatically by a computer via a serial port. The focal plane scanner performs line scanning across an input imaging area within the focal plane of the front lens, which was done by the aircraft or the satellite movement in the airborne configuration, and the spectrograph disperses each line into a spectrum and projects a two-dimensional image profile (line image) onto the CCD surface.

Many hyperspectral scanners have being modified for laboratory applications. The most advanced and the one related to our subject of interest is the one developed in the Laboratory of Biomedical Imaging at the University of Texas at Arlington, based on a prototype developed at the National Institutes of Health, Bethesda [9]. They developed a multimodal reflectance hyperspectral imaging system for imaging in

the visible and the near infrared using liquid crystal tunable filters for spectra band selection with improved performance in clinical and surgical applications. They used two separate cameras for imaging in the visible region and near-infrared region.

The CoolSNAP$_{ES}$ monochrome camera is used for the visible range imaging, which incorporates a SONY ICX-285 silicon chip. The camera has a digitizing speed of 20 MHz and hence provides high speed and high sensitivity over a 1329 x 1040 imaging array. The PIXIS 400BR, a fully integrated system with permanent vacuum/deep cooling from Princeton Instruments, is used for the imaging application in the near infrared region. The PIXIS 400BR camera incorporates a digitization speed of 100 KHz to 2 MHz.

The system uses a liquid crystal tunable filter (LCTF) (Cambridge Research & Woburn, MA), which provides compact, electronically tunable, spectral bandpass filters with imaging capabilities filtering only a single narrow bandwidth of light at a time, providing rapid selection of any wavelength in the visible and NIR region [10].

Electronically tunable filters are used for spectral imaging because they can provide transmittance at varying wavelengths and bandwidths by controlling the crystals either by acoustic signals or voltage [11].

The LCTF is built using a stack of polarizers and tunable retardation (birefringent) liquid crystal plates forming the LCTF element. The selection of a particular frequency and the pass band around it is done by applying voltage to the quartz crystal.

Another form of tunable filter is the acousto-optical tunable filter (AOTF), in which a single wavelength of light is separated using radio frequencies (RF) or acoustic waves. The wavelength of light selected is a function of the frequency of the

RF signal applied to a Tellurium Dioxide (TeO$_2$) or Hg$_2$Cl$_2$ crystal. The AOTF uses an RF transducer that emits acoustic waves.

The acoustic waves pass through the Tellurium Dioxide crystal and cause the lattice structure to be alternately compressed and relaxed. The resultant density changes produce refractive index variations that act like a transmission diffraction grating or Bragg diffracter. The AOTF only diffracts one specific wavelength of light, so it acts more like a filter than a diffraction grating.

The latest development in this area, which is more efficient in terms of response time, uses a programmable digital micromirror device (DMD) from Texas Instruments DLP Products [12]. The new system has a DLP DMD-based spectral illumination light source. The OL-490 is developed by Optronic Labs. In the DMD source, broadband light is diffracted through a slit, reflected from a grid of digitally-controlled programmable micromirrors, and optically directed to a focal plane array (FPA) or digital camera sensor through a liquid light guide (LLG), similar to an optical fiber with an increased capacity for transmitting light. By controlling the state of each mirror individually, the source illuminates tissue with a programmed selection of light wavelengths, and the camera measures the reflection of that spectrum. The use of mirrors instead of liquid crystal tunable filters makes the DMD hyperspectral imager's tuning time faster and the wavelength range broader.

The DMD hyperspectral imager operates in two illumination modes to assess tissue oxygenation: 'Sweep' and '3shot'. In 'Sweep' mode, 126 discrete wavelength scans with 10 nm bandwidth are used to acquire 126 images of the hyperspectral data, which is similar to filtering broadband white light using the LCTF system. After acquiring the images, the spectral signatures of oxyhemoglobin (HbO$_2$) and deoxyhemoglobin (deoxy-Hb) track the oxygen content in the blood in order to color-code each pixel. One color coded image is generated every 20 seconds. In the '3shot' method, the DLP source is used to illuminate the tissue with color mixtures of light

chosen to reveal differences between the known spectral signatures of oxyhemoglobin and deoxyhemoglobin.

The approach taken to assemble the hyperspectral imager using optical filters is not a novel approach. Attempts to build similar models have being made already, but building a complete apparatus gives the freedom to design the apparatus according to our requirements.

1.3.   Proposed approach

The proposed approach in this thesis is to use bandpass optical filters that are able to transmit light from a particular band to get images of the subject of interest. These filters must be sequentially selected and placed in front of the camera. Placing the filters in front of the camera manually while taking multi/hyperspectral images would be a tedious job. Therefore, the optical filters will be mounted using step up rings glued to the holes in a rotating disc, making the optical filters with c-mounts easily detachable. The disc will then be rotated with the help of a stepper motor so that an image can be captured from every filter on the disc without any user intervention. The entire process of capturing images can to be completed in a minimum amount of time by rotating the disc at high speed, and the illumination could be considered as constant through the short interval.

Ten optical filters chosen are mounted on the disc. The raw images from the image acquisition step will be processed to make them usable for further analysis. The images must be corrected for the uneven response of the camera, the light source and the optical filters. Gray card correction is also implemented using piecewise linear stretching. The proportion of incident photons transmitted through each optical filter is not equal, causing the image intensity levels to shift. To correct for the shift, the intensity levels in the images are normalized using the area under each filter response. This processing will prepare the images for analysis, and the difference in the intensity

levels in the 10 images will depend only on the reflectance property of the material under study.

1.4.   Organization of the thesis

This thesis report concentrates on the design of the apparatus and its automated operation for processing the images for physiological analysis.

The thesis is divided into four chapters. The first chapter deals with the introduction to multispectral and hyperspectral imaging, specifying the objective and discussing some previous work done in terms of modifying the camera to take multispectral images.

The second chapter deals with the mechanical components and the electronics required to employ the apparatus design so that it can be moved in synchronization with the camera.

The third chapter goes through the image processing steps taken to make the images suitable for analysis, correcting illumination, camera response and the filter responses. Image registration was also implemented to correct any shifts or deflections due to subject movement.

The final chapter deals with the approaches taken for data analysis of hyperspectral images that can be carried out for classifying and identifying substances with known spectral signature from the entire image, i.e. identification of degenerated tissues from the healthy ones according to the blood flow available to them. In conclusion, we discuss some criteria that should be undertaken for better results using the apparatus.

CHAPTER II

MECHANICAL ASSEMBLY

The thesis develops an easy and efficient method of capturing images using different frequency bands of light. These images at different frequencies of light are captured using optical filters having different frequency passbands. To accomplish this, a electro-mechanical apparatus is required that can rapidly change the optical filters in front of the camera, capture images, and store them in their raw state for further analysis. These images must be taken rapidly so that all images are taken under similar lighting conditions, with minimal movement of the subject of interest.

Images at 10 different frequency intervals were taken using 10 different optical filters. Each filter was chosen so the center frequencies are well separated and minimal overlap exists between the light passbands. High transmittance in the passband region and almost zero transmittance in the stopband region was another important criterion. These optical filters are mounted on a circular disc that is rotated with a motor so that the images can be taken through all the filters in a single sequence without interruption or any user intervention.

The final component of the assembly was a separate control on the light, i.e. the light source incidence can be controlled manually to provide better illumination of the object of interest according to the distance of the object from the light source.

2.1. Structural Components

The smooth and quick capture of images with this concept requires a rotating disc on which to mount optical filters. This mechanical design allows images to be captured in quick succession, creating a stack of images taken at different frequencies for a particular state of lighting and subject of interest.

2.1.1.   Metal work

A 3/16" thick aluminum plate of 12" x 12" was selected as a base plate. A 3/8" thick aluminum plate of 12" x 12" was selected to mount the optical filters.

The design requires fitting the wheel with 10 optical filters. One orifice was left unfilled to act as the all pass filter. Twelve orifices were made for the sake of symmetry, and two orifices were left unoccupied.

Figure 4 shows the dimensions of the disc with the 2.18 inch orifices and an additional hole for the motor shaft, with a shaft key to hold on the disc to the motor.
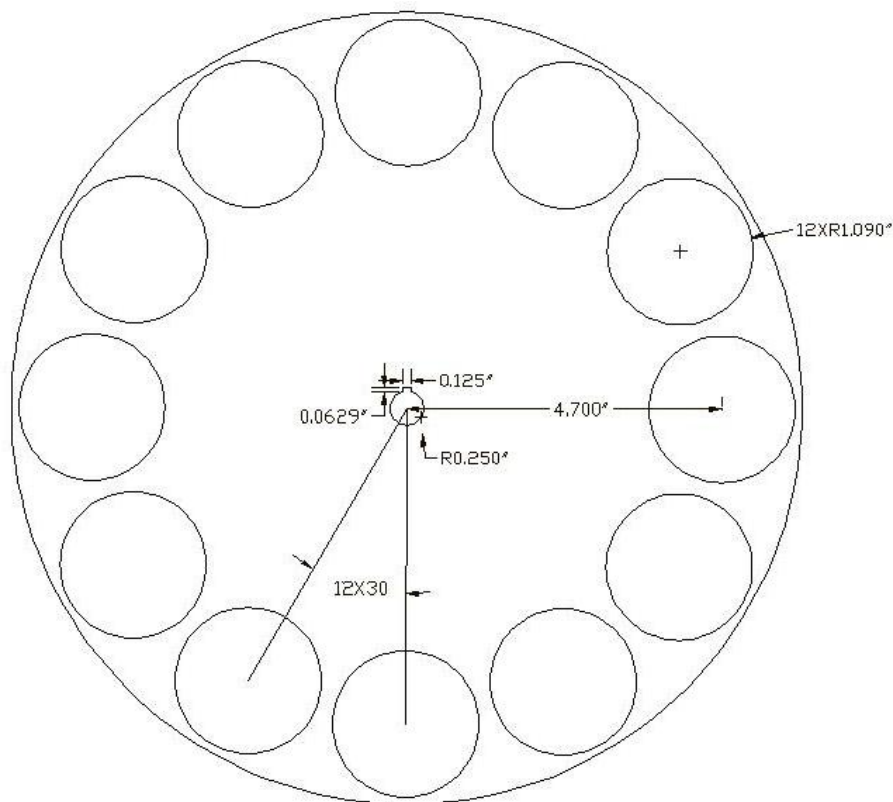
Figure 4. Optical filter mounting disc with dimensions

Figure 5 shows the disc in the 3D format, generated in Autodesk Inventor 2008 through an ".ipt" file, which was required to cut the disc in the required shape on the CNC machine.
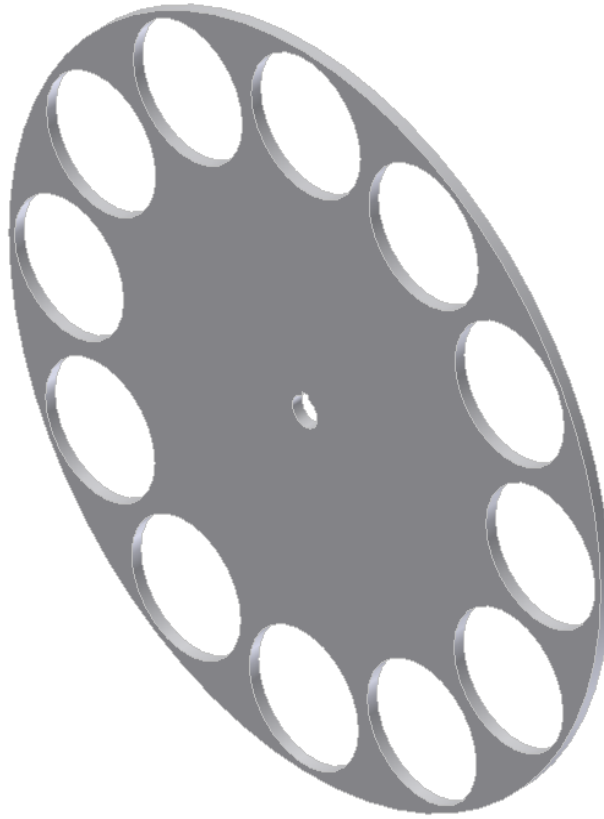
Figure 5. 3D view of the disc in Autodesk Inventor 2008

Figure 6 shows the top view of the base plate with the position of the motor (shown by dashed line). The holes are shown with their required threading for the screws to fasten the support blocks for the motor mounting plate, the camera lens mount and the vibration damping studs. The vibration damping studs are used to reduce vibration effects while the disc is in motion so that the apparatus is steady while capturing images.

The list of the structural components required for the assembly are as follows:

Table 1. Bill of materials

Disc plate	Aluminum plate, 3/16" thick, 12" x 12"
Base plate	Aluminum plate, 3/8" thick, 12" X 12"
Plate to mount motor	Aluminum plate, 3/8" thick, 4" width, 12" length
Support for the base plate	Heavy−duty vibration damp leveling mount, with stud, 3/8"−16 thread, 35 # max load
Support for the motor mount plate & lens	Aluminum plate, 1" square, 12" length
Key for motor shaft	Zinc-plated steel undersized key stock 1/8" X 3/16", 12" length
Filter holder	Tonika stepping ring 49 mm-52 mm, TOK 49/52, 11 piece Threaded filter holder for 2" square filter, 2 piece Fotodiox 52 mm to 58 mm filter thread, 52-58 mm macro close-up Reverse coupling ring, anodized black metal ring, 2 piece
Screws, nuts and washers for support	Zinc−plated steel pan head phillips machine screw, 12−24 thread, 1" length Zn−plated steel machine screw hex nut, 12−24 thread, 7/16" width, 5/32" height Zinc−plated steel pan head phillips machine screw, 12−24 thread, 2" length 100D flat head phillips machine screws, 300 series SS, 8−32 thread, 1" 1" length Zinc−plated steel machine screw hex nut, 8−32 thread, 11/32" width, 1/8"height Cadmium−plated steel MIL spec flat washer, 10 size, No. 8, .219" ID, .438" OD, .036"−.065" thick Zn-plated steel flat head philips machine screw 8-32 thread, 2-1/2" length, packs of 50
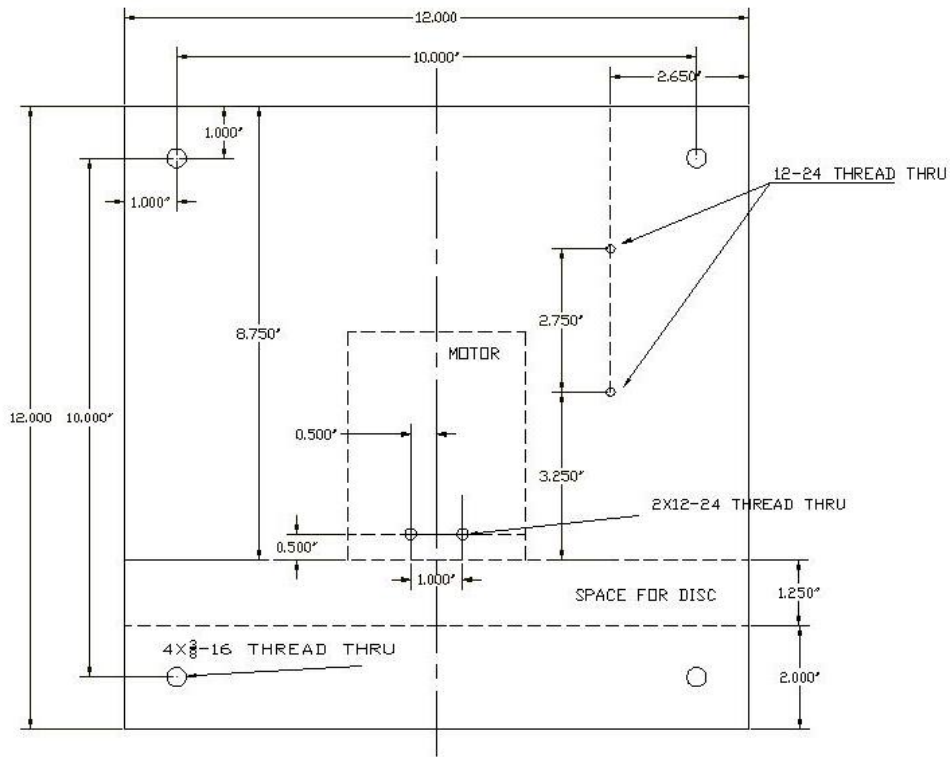
Figure 6. Base plate with dimensions

The base plate was purchased with the required external dimensions, so it only required drilling and threading holes to attach other metal components using nuts and bolts. These holes were cut on a simple milling machine, where the threading was also done.

The damping studs used heavy duty vibration-damping leveling mounts, with the stud having a flange nut and a hex nut for height adjustment. These mounts have a black neoprene base bonded to a threaded steel insert, which facilitates better damping of vibrations.

The support blocks are 1" × 1" × 4" inch thick rectangular blocks, with threaded holes to align the lens and the motor mounting plate.
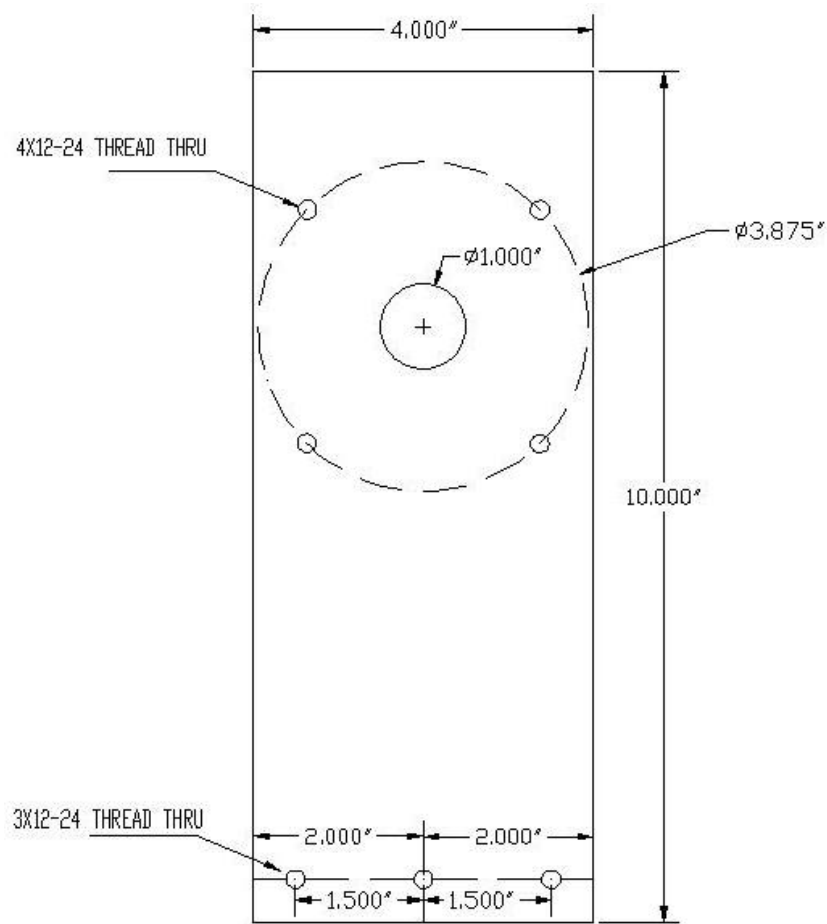
Figure 7. Motor mounting plate with dimensions

The motor mounting plate shown in Figure 7 is a 3/16" thick aluminum plate of 4"x10". The length of the mounting plate was intended to be 10", so that the disc when mounted on the motor attached to the plate has good clearance from the base plate. This spacing provides room to mount the home switch, which positions the disc at a particular starting position at the beginning of every new session. The home switch operation will be explained in the next subsection.

The motor mounting plate has threaded holes for screws to attach it to the support and the motor. Four holes lie on a circle for the motor attachment, and a one inch diameter hole serves as a clearance for the motor shaft.

2.1.2. Optical filter and filter mounts

The optical filters chosen to capture images at different frequency bandwidths are spread along the visible and the near-infrared spectrum. This current set of filters makes the assembly applicable for multispectral imaging. The following Table 2 shows the central frequencies of the 10 optical filters, and their frequency responses are shown in Figure 8.
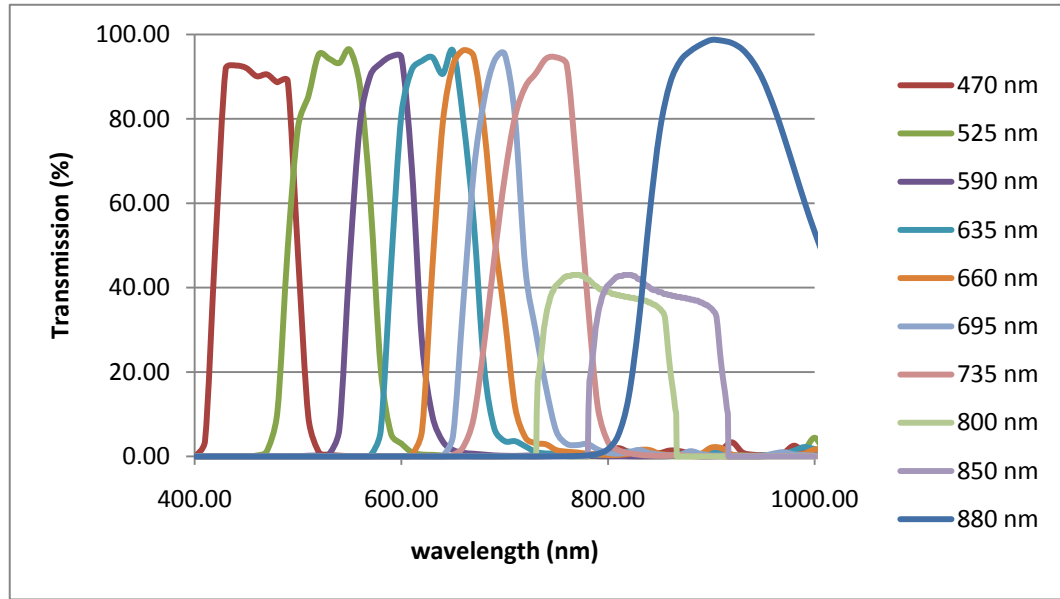
Figure 8. Response of the optical filters

Table 2. Central frequency of optical filters

FILTERS	1	2	3	4	5	6	7	8	9	10	11
λ (nm)	All pass	470	525	590	635	660	695	735	800	850	880

A 49-52 mm step up ring (Tiffen Company, Hauppauge, NY) is glued to each orifice to attach the optical filters. The step up rings were chosen so that the filters can be easily replaced without threading the inner side of the orifices. The step up rings are glued to the orifices on the metal plate using a general purpose epoxy.

The optical filters with central frequency 800 nm and 850 nm are square shaped. A 52-58mm macro close-up reverse coupling ring (Fotodiox Inc., Waukegan, IL) is used to attached the 2" Square Threaded Filter Holder (Edmund Optics Inc., Barrington, NJ) shown in Figure 9 to the glued 49-52 mm step up ring.

Figure 9. 2" Square threaded filter holder [13]

2.1.3.   Final Product

The final structural apparatus can be seen in the following figures, showing different views of the entire assembly.
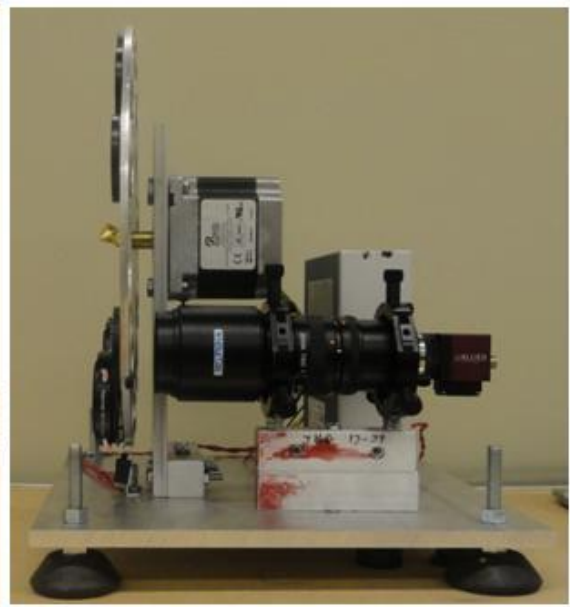
Figure 10. Views from all 3 directions of the apparatus

2.2.   Electrical Components & Programmed Control

2.2.1.   Electrical Components & Connections

The main electrical component required for the assembly is the motor. Every other component is for controlling the motor, which rotates the disc and holds it steady at a particular position.

Table 3 shows the electrical components required to implement the mechanical assembly.

Table 3. List of electronic components

COMPONENTS	
1	N31HRLG-LNK-NS-00 stepper motor, NEMA 34, 610 oz-in, single shaft
2	P70360 stepper drive, 120 or 240 VAC powered, 2.5 A continuous current, 1 axis
3	UMI-7764 (20 MHz Encoders) 4-axis motor wiring connectivity cable
4	D-sub to leads cable for P70530 & P70360 stepper drives, 2.5 m
5	SHC68-C68-S, 68 pin VHDCI to 68 pin VHDCI cable, 0.5 m
6	NI PCI-7332 low cost 2-axis stepper only controller

These components were purchased from National Instruments, Austin, TX. The decision to purchase these from one vendor facilitated compatibility of different equipment.

The motor was chosen according to the torque required to move the disc. It provides a very high holding torque, so that the disc is steady and precisely placed while images are being captured.

Figure 11 shows the connections of the electronic components for the assembly.
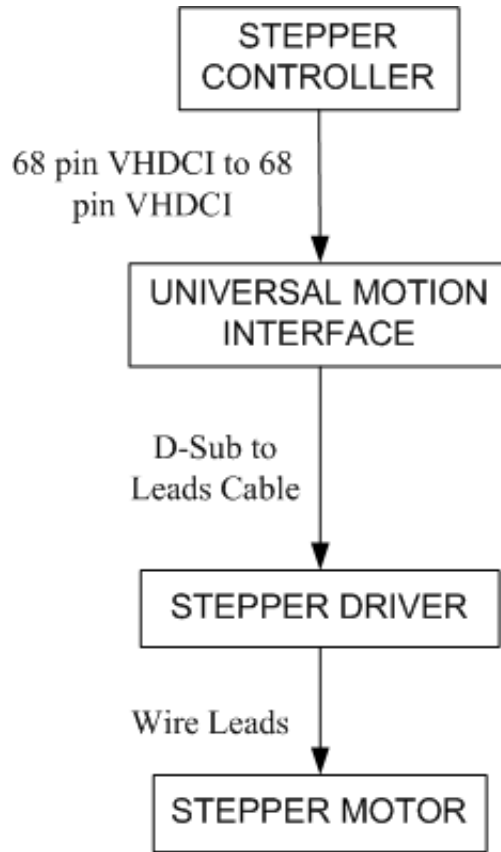
Figure 11. Connections of the Electronic Components

The connection between the stepper motor and the stepper drive by means of the leads provided on the motor to the J6 connector on the drive is shown in Figure 12.
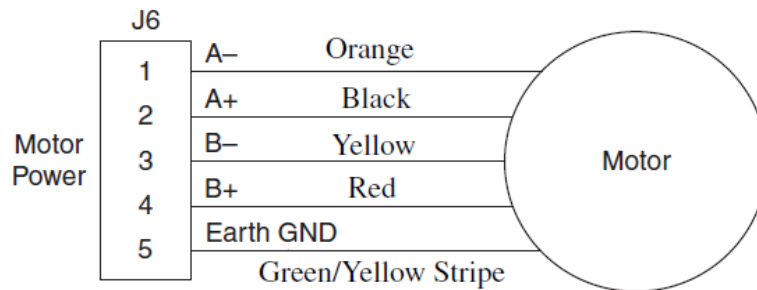
Figure 12. Connections from stepper motor to stepper driver [14]

The set switches S1 and S2 are used to configure the motor drive. The switch S1 determines the model of the motor connected; the set of S2 (1-12) switches determines the settings for motor control. The function of each S2 switch is listed in the Table 4.

Table 4. Function of DIP switches on drive

SWITCH	FUNCTION
S2-1	OFF position for the P70360 drive
S2-2	Step Resolution
S2-3	
S2-4	
S2-5	Load Inertia
S2-6	
S2-7	
S2-8	Dynamic Smoothing
S2-9	
S2-10	Current Reduction
S2-11	Multistepping
S2-12	Encoderless Stall Detection

The positions of the DIP switches on the stepper driver for our purpose are shown in Figure 13.
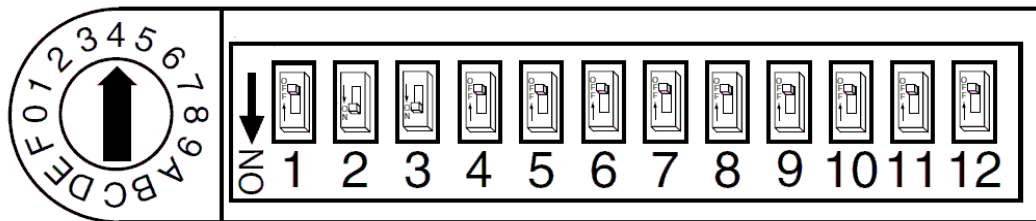
Figure 13. DIP switch positions [14]

The UMI-7764 is connected to the driver using the D-sub connector on the driver side and leads connected to the UMI. The D-Sub to Leads Cable has color

coded wires to connect to one of the axes on the UMI. Figure 14 shows the connections on AXIS1.
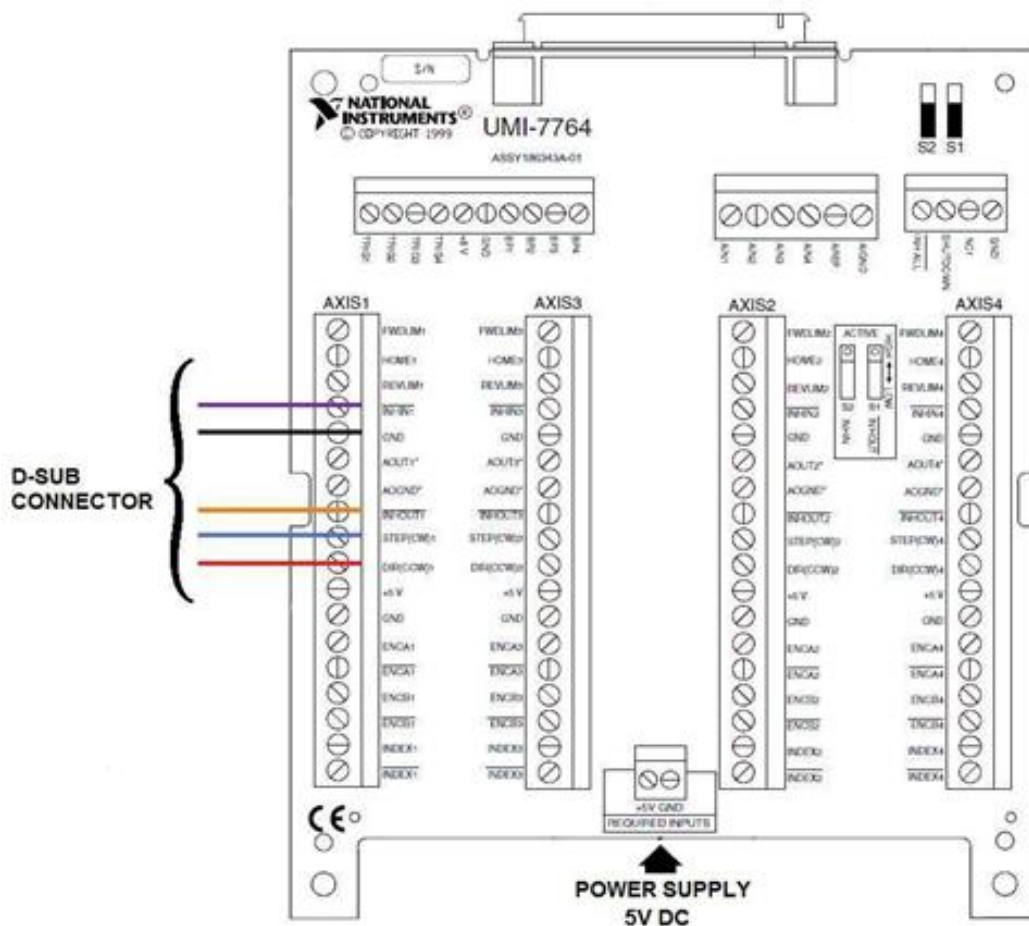
Figure 14. Connections on UMI-7764 [14]

The UMI is powered using an AC adapter, producing output of 5 V DC and current of 1000 mA.

The UMI-7764 is connected to the NI PCI-7332 stepper controller using a 0.5 m long cable (SHC68-C68-S, 68 pin VHDCI to 68 pin VHDCI).

2.2.2. Motor Control

The motor is controlled using '.dll' (dynamic link library) files generated in LabVIEW and run in MATLAB because the equipment was purchased from National Instruments, and it could be easily programmed in LabVIEW.

The rotation sequence was programmed in LabVIEW. Different speeds were chosen while rotating the wheel to find the home position and while taking images. Figure 15 shows the graphical code for the motor control.
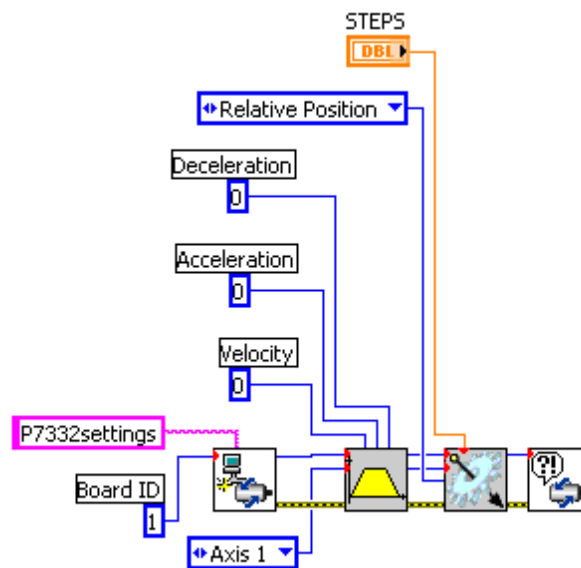
Figure 15. LABVIEW VI code for moving the motor

Figure 15 shows the code to move the motor in LabVIEW. This code requires the user to input acceleration values in the spaces below Deceleration and Acceleration in change of steps per second and to input speed below Velocity in terms of steps per second. Relative Position suggests that the number of steps to be taken is counted from the present number of steps and not according to the absolute location.

This LabVIEW code is then converted into ".m" MATLAB function and linked to the LabVIEW libraries through the ".dll" files created using the NI LabVIEW Math Interface Toolkit (MIT), which enables calling the LabVIEW VI from MATLAB.

For smooth movement of the motor and stability at high speeds, the motor was set to take micro steps (18000 steps per revolution) rather than full steps (200 steps per revolution).

2.2.3. Camera and its control

The image acquisition process is accomplished using a monochrome camera with a large dynamic range and a wide spectral bandwidth. A monochrome camera with a frequency response from 400 nm-1000 nm was selected rather than a color camera.

The camera is a Guppy F-146B (Allied Vision Technologies GMBH, Germany). This monochrome camera offer an IEEE 1394a interface, 12-bit (4096 levels), maximum picture size of 1392x1040, with a frame rate of 17.7 fps at maximum resolution, and a high transfer rate up to 400 Mbps. The sensor of the camera is a charge coupled device (CCD) with favorable characteristics across the required wavelength region.

The camera is controlled using CMU 1394 Digital Camera Driver version 6.4.5 [15], which is compatible with Windows® XP and all lower versions. The GUI of the CMU driver provides a graphical interface to control the settings of the camera. The Image Acquisition Toolbox of MATLAB is used to control the camera with the CMU driver. A simple sequence of functions enables capturing the images in their 12-bit raw format.

Table 5 tabulates the specifications of the Guppy F-146B camera, shown in Figure 16.

Table 5. Camera specifications [16]

Specifications	Guppy F-146B (b/w)
Image device	Type 1 (diag. 8 mm) progressive scan, SONY IT CCD ICX267AL
Picture size	Up to 1392 x 1040 pixel
Cell size	4.65 μm x 4.65 μm
Resolution depth	12 bit (12 bit ADC)
Lens mount	C-Mount, CS-Mount (convertible via adapter)
Digital interface	IEEE 1394a (IIDC V1.3), single port
Transfer rate	100 Mbit/s, 200 Mbit/s, 400 Mbit/s
Frame rates	Up to 17.7 fps (full frames)
Gain control	Manual 0-24 dB (0.035 dB/step); auto gain (select. AOI)
Shutter speed	40 μs…67s; auto shutter (select. AOI)
External trigger shutter	Programmable, trigger level control, bulk mode (1 trigger, n shots), programmable trigger delay
Smart features	AGC (auto gain control), AEC (auto exposure control)
Power requirements	8 V – 36 V DC via IEEE 1394 cable or 8-pin HIROSE
Power consumption	Less than 2 watt (@ 12 V DC)
Dimensions	48.2 mm x 30 mm x 30 mm (L x W x H), w/o tripod and lens
Mass	50 g (without lens)
Operating temperature	+5… + 45° Celsius without condensation
Storage temperature	-10… + 60° Celsius without condensation
Regulations	CE, FCC Class B, RoHS (2002/95/EC)
Options	Board level version, power out (HIROSE), AVT FirePackage / Active FirePackage / Fire4Linux

Figure 16. Guppy F-146B camera

Figure 17 shows the response of the camera over 400-100nm, which is sufficient for the requirements of the project.
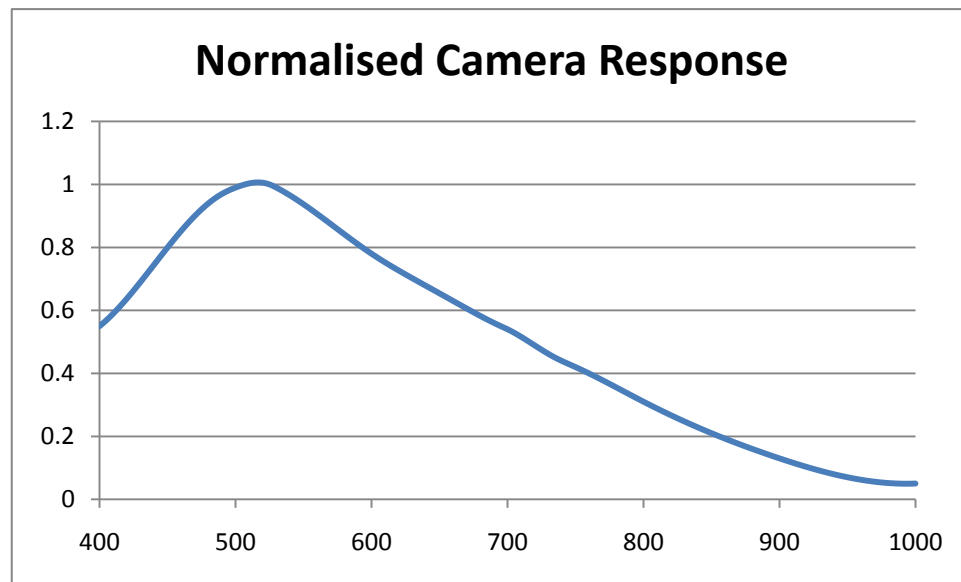
Figure 17. Camera response

The collecting optics consists of a typical camera lens. The Zoom 7000 lens (Navitar Inc., USA) shown in figure 18, is used before the camera for magnification and to increase the range of image capturing. The Zoom 7000 offers a 6X

magnification power over a focal range of 18 mm to 108 mm. The camera provides a C-mount extension by which the lens is fitted to the camera.

Figure 18. Navitar Zoom 7000 lens

The lens is supported using an adjustable radius lens chuck (Newport, Irvine, CA), shown in Figure 19. It facilitates adjustment of the lens, vertically and horizontally, to be placed right behind the empty orifice when the disc is in the home position.

Figure 19. Adjustable radius lens chuck

2.2.4. Home switch

The home switch is a simple SPDT lever switch, shown in Figure 20. This switch is positioned such that it changes to the ON state on contact with a small peg glued to the disc, marking a pre-calculated home position. The leads of the switch are connected to the AXIS 1 of UMI-7764, as shown in following Figure 21.

Figure 20. SPDT home switch
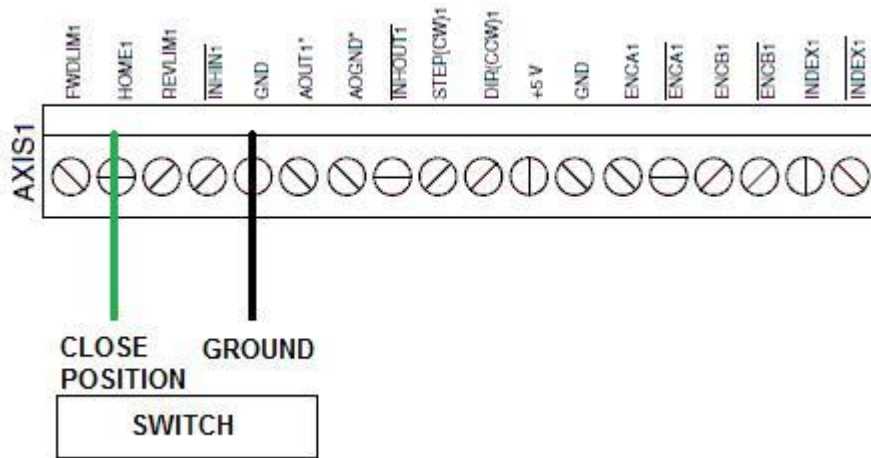
Figure 21. Home switch connection [14]

2.2.5. Light source

The frequency range of the last three optical filters is in the near-infrared region. To have good images through these filters, a light source capable of emitting

light further into the near infrared band was chosen. The light source selected produced light across frequency range from 400 nm - 2100 nm.

The light source selected from Illumination Technologies, Inc. (Syracuse, New York) uses an EKE-ER Lamp, 150 W, with 21 V DC regulated output. The power switch, the intensity control and the fiber optic receptacle are located on the front panel. The thumbscrew, located on the receptacle, locks a fiber optic light guide into the proper position. The light intensity of the lamp varies with the intensity control knob setting. Typical values are shown in table 6.

Table 6. Lamp intensity for corresponding knob position [17]

Knob Position	Lamp Voltage (V)	Lamp Intensity (%)
1	3.4	0.19
2	4.9	0.94
3	6.4	2.74
4	8.4	7.54
5	10.7	16.40
6	12.9	29.41
7	15.4	49.41
8	17.3	69.41
9	18.9	88.24
10	19.8	100.00

The life span of the lamp depends on the intensity at which it is used. A modest reduction below full intensity in the setting will dramatically increase the service life of a lamp.
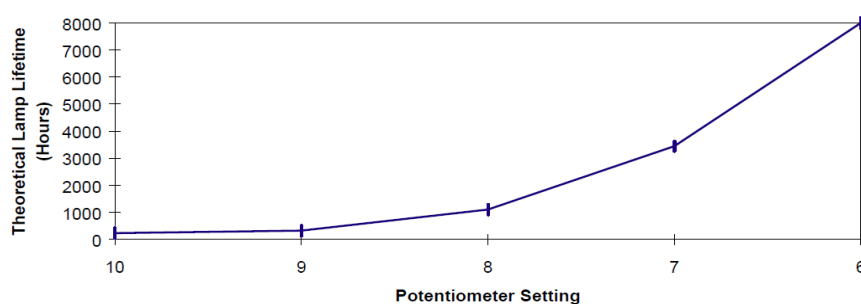
Figure 22. Graph showing intensity knob settings vs lamp life (hours) [17]

31

Figure 22 shows a plot of intensity setting vs. lamp lifetime. Table 7 lists the lamp lifetime and the lamp voltage at the corresponding knob position.

Table 7. Life of lamp (hrs) for corresponding knob position [17]

Knob Position	Lamp Voltage (V)	Lamp Life (hrs)
1	3.4	Approximately 8000
2	4.9	Approximately 8000
3	6.4	Approximately 8000
4	8.4	Approximately 8000
5	10.7	Approximately 8000
6	13.6	Approximately 8000
7	15.8	3441
8	17.7	1105
9	20	326
10	20.7	231

Figure 23 shows the front panel of the light source and the optical light guide, with the flexible stainless steel sheath used. Figure 24 shows the light response.
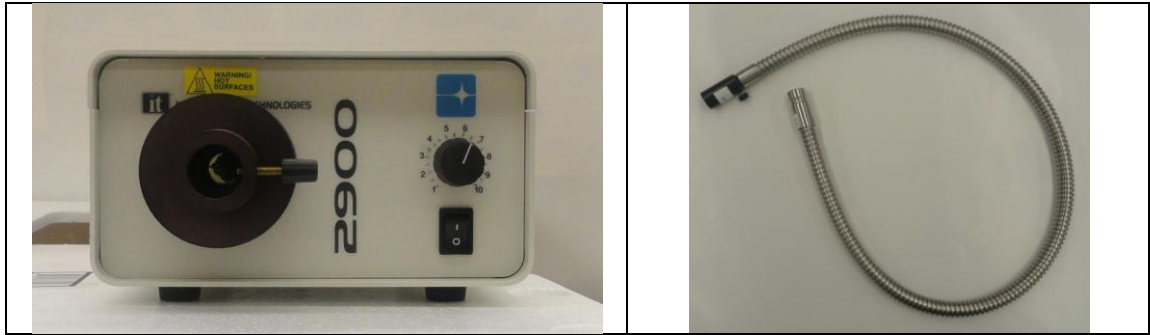
Figure 23. Light source and the light guide

The light source is connected to an adjustable gooseneck desk lamp through a fiber optic light guide, as shown in figure 25, so that it can be adjusted to be in any position to illuminate the subject of interest.

Normalized Light Response
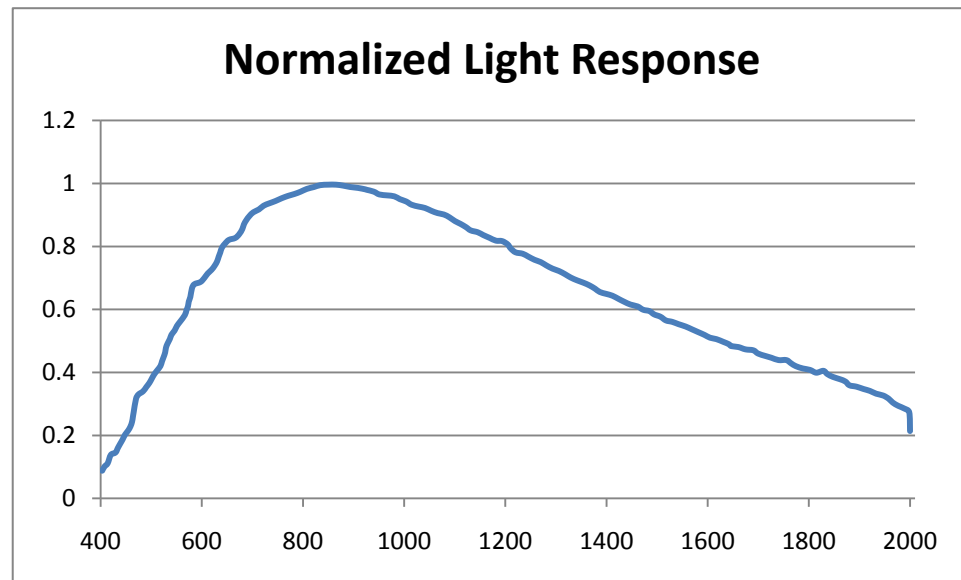
Figure 24. Light source response
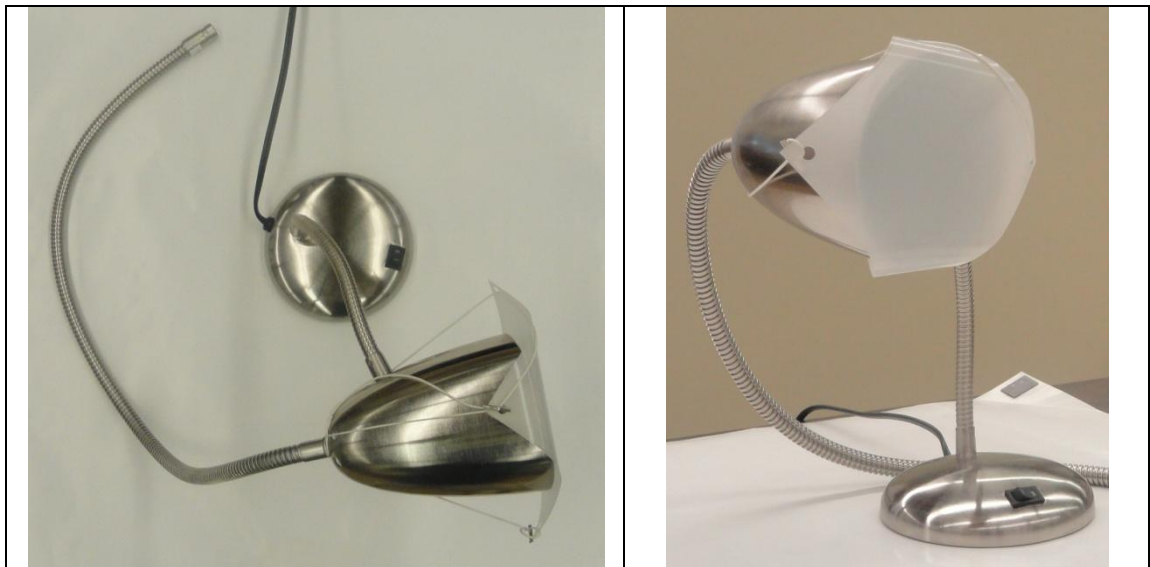
Figure 25. Gooseneck lamp setup for the light source

Diffusers are used to cover the lamp, as shown in figure 25, in order to scatter the light and avoid direct incidence of light that might result into saturation of images. Diffuser film is a one sided film (Anchor optics, Barrington, NJ) designed to break up and distribute light evenly, providing 87% transparency and greater flexibility.

2.3. Image acquisition

The basic process flow for image acquisition can be seen in the following flow chart.
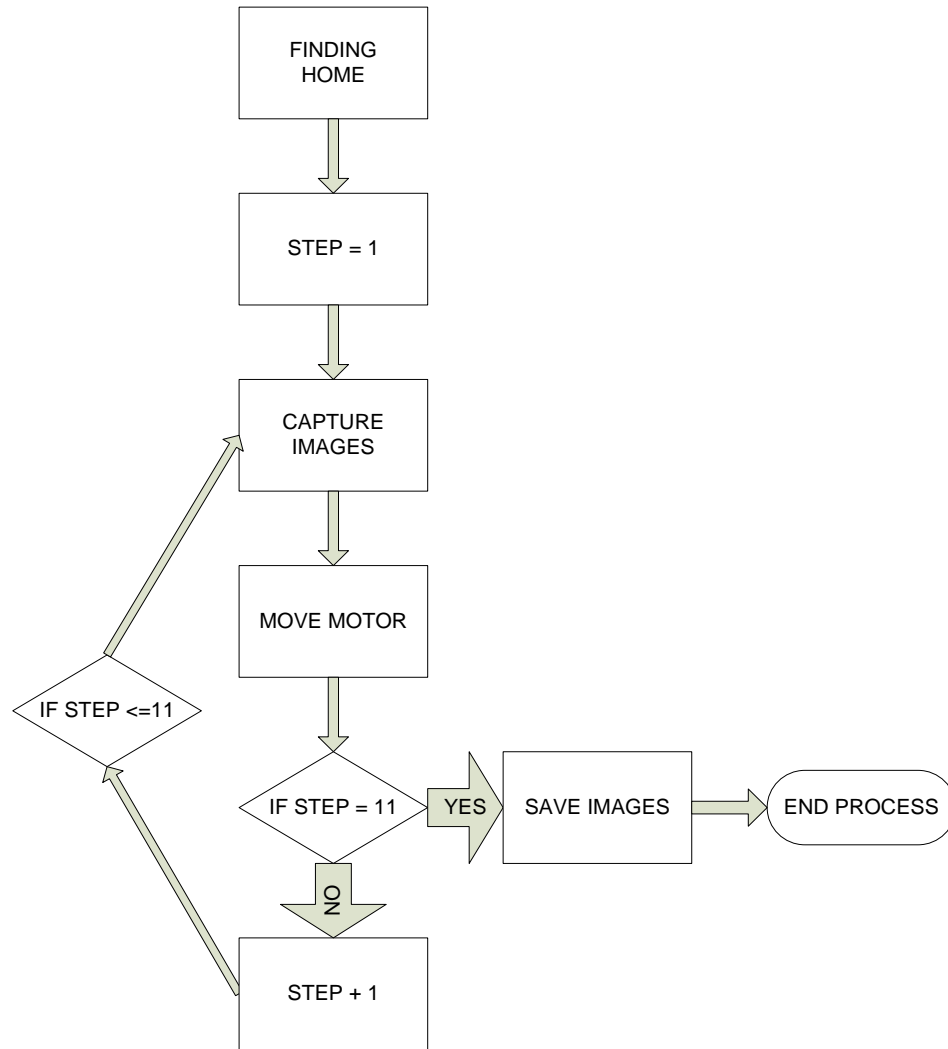
Figure 26. Image acquisition process flow

The home position of the disc is selected such that the empty orifice is in front of the lens. Finding this home position is a mandatory step before starting the image acquisition process.

The image is captured from the empty orifice first and then through the 10 optical filters. This process requires an 11 step loop, shown in Figure 26, of image capture and disc movement to the next optical filter. All the 11 images are then saved in their raw state in MATLAB's ".mat" matrix format.

The image acquisition step is carried out through a synchronous process using the mechanical and electrical components previously described to capture and store the raw spectral images for further processing and analysis.

CHAPTER III

IMAGE PROCESSING AND ILLUMINATION CORRECTION

In this chapter we will discuss the processing required for the raw images captured from the acquisition step. These images must be processed to make them usable for further analysis.

3.1.   Equipment response calibration

The light source, the camera and the filters do not have a flat response. Thus, the intensity levels that are seen in the images are not solely due to the reflectance property of the subject of interest but also because of the uneven response of the equipment. This unwanted response characteristics must be corrected in order to get images to enable determination of reflectance characteristics. In order to achieve this goal, light source and camera response correction is applied first. The correction is applied across the range of 400 nm to 1000 nm.
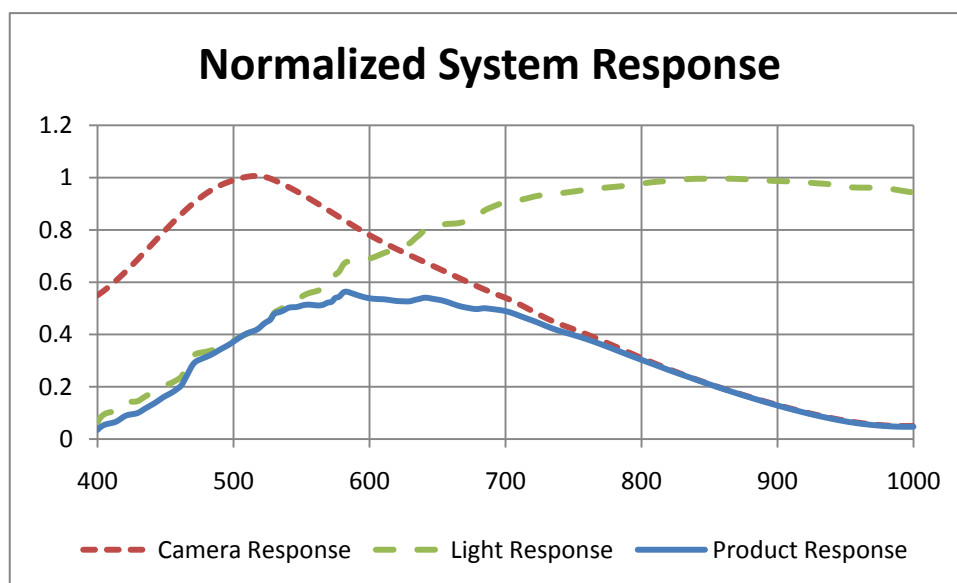
Figure 27. Product of the light and camera response

The system response of the light source and the camera can be seen in figure 27. This system response is then used to correct with the optical filter response. Because we use one optical filter at a time, 10 different calibration constants are required.

The normalized system response is multiplied with each of the filter responses. The effective bandwidth of each filter is defined using the full width half maximum (FWHM), where the width of filter response reaches half its maximum value, at -3 db attenuation. The product of values from the normalized system response and the filter response are averaged within the range as shown by different colors for each filter in Figure 28. The mean value from all the filters is used to calculate the calibration constant, which will take the responses of all the filters approximately to the maximum mean value.
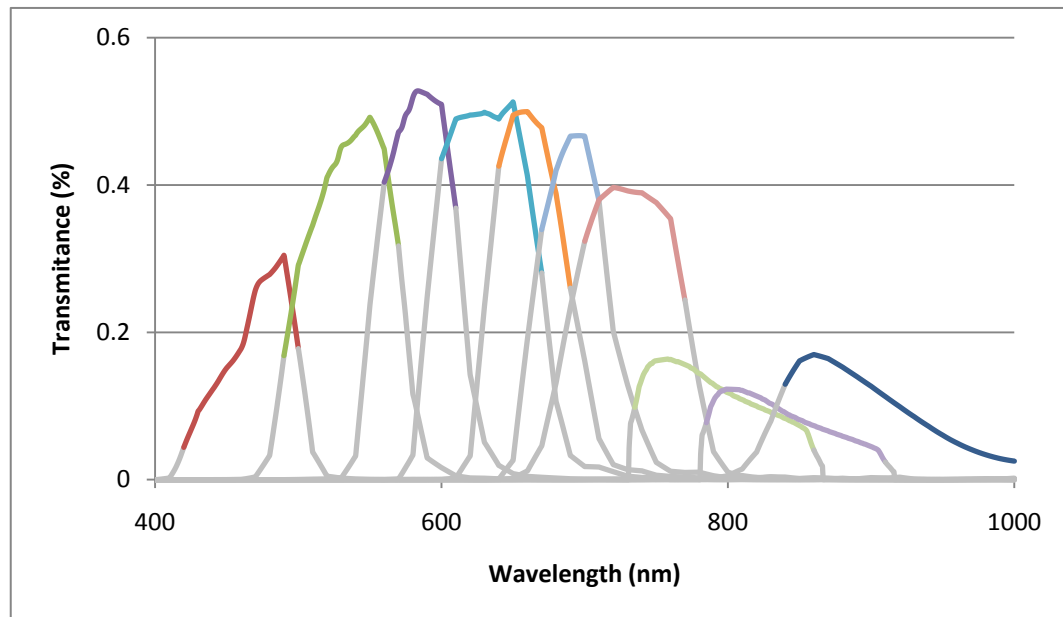
Figure 28. Plot showing top 50% of peak transmittance of filters

The original images acquired were 12-bit images, but after the correction is applied according to the calibration constants, the resulting gray level values could be

larger than 4096. The image intensity values are allowed to increase, causing each image to have different dynamic range, and further processes are carried out on these extended gray level images. The following table gives the calibration values for the 10 filters.

Table 8. Calibration constant for images

Filter	λ (nm)	Calibration
1	All pass	NA
2	470	2.4070
3	525	1.1514
4	590	1.0052
5	635	1.0000
6	660	1.0670
7	695	1.1417
8	735	1.2937
9	800	3.7549
10	850	5.3193
11	880	4.5223

Table 9. Compensation factor for the filters

Filter	λ (nm)	CF
1	All pass	NA
2	470	1.5600
3	525	1.5984
4	590	1.2623
5	635	1.5968
6	660	1.2498
7	695	1.1750
8	735	1.6488
9	800	1.0000
10	850	1.0000
11	880	2.9411

The response of all the filters is different, so that the proportion of the incident photons transmitted through each filter is not equal. This unequal transmittance of photons affects the intensity levels in the image due to the different number of photons reaching the camera to form the image. To compensate for this irregularity, the intensity levels are divided by the normalizing factor that takes the area under all the filter response curves, equal to the smallest area among the 10 filters. Table 9 shows the compensating factor (CF) for each filter.

The corrections for the light and the camera response and the compensation factor to normalize the proportion of the incident photons were made together before capturing the images, changing the camera gain for every image. The gain values are calculated by the following formula.

$$Gain = \frac{Calibration\ values}{compensation\ factor} \qquad \dots (1)$$

Table 10 shows the gain specified for all images.

Table 10. Gain for the images

Filter	λ (nm)	Gain
1	All pass	1
2	470	1.5429
3	525	0.7203
4	590	0.7963
5	635	0.6263
6	660	0.8537
7	695	0.9717
8	735	0.7846
9	800	3.7549
10	850	5.3193
11	880	1.5376

This method corrects for the response unevenness and the proportion of incident photons even before the images is formed, avoiding round off errors when the images are processed.

3.2.   Gray card correction

Correction for the perceived intensity was done using a gray card capable of generating peaks at three different gray values i.e. white, middle tone (gray) and black. According to the gray card specification, these shades of gray should lie in the range specified in table 11.

Table 11. Range of the three shades on the gray card

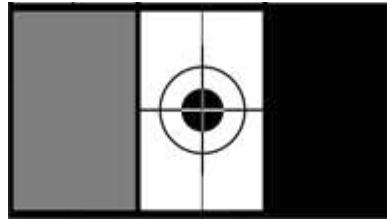| Levels	BLACK			50% GRAY			WHITE		
	-3σ	Peak	+3σ	-3σ	Peak	+3σ	-3σ	Peak	+3σ
256	20	50	70	105	128	151	225	235	245
4096	320	800	1120	1680	2048	2416	3600	3760	3920

Figure 29. Gray card

The gray card response is specified according to 256 gray levels, but these will be stretched and shifted for a camera capable of providing greater resolution in terms of gray levels. The entries corresponding to the 4096 levels in Table 11 shows the possible position of the three modes from the gray card when imaged from a 12 bit camera.

This linear stretching and shift is achieved using piecewise-linear stretching. To implement this linear stretching, first we find the peaks of the modes in the histogram of the gray card image seen in Figure 29 and also the stretch of the three modes.

The specification of the gray card is for the all pass image, so the linear stretching to be applied must be calculated from the all pass image. The detection of the stretch of the modes is carried out on the images captured through all the filters, and corresponding stretching to be applied to the spectral images is calculated from the all pass image and the entries in the Table 11.

The first step in the peak detection process is to get a smooth plot from the histogram. A simple smoothing function might have also sufficed to smooth the plot, but that could cause the peaks to shift along according to the span of the convolution function used. To avoid this, the histogram was fitted with a one dimensional Gaussian mixture model to get a smooth looking plot with no shift in the location of the peaks. The algorithm for Gaussian mixture model divided the data into equal parts according to the specified number of Gaussians. These different groups of data were fitted with Gaussians in an iterative process. For better fit to the histogram, more than 3 Gaussians were used. This algorithm converged quickly because the peaks were well separated in most of the cases. The output of the Gaussian mixture model fitting procedure gives the mean and the standard deviations of the Gaussian distributions. Figure 30 shows a histogram fitted with Gaussian mixture models.

Peak detection was then performed using a derivative method on the Gaussian fitted model to detect the peaks. The distance between the means of the Gaussians and the peaks of the modes was used to determine which modes formed by the gray shades were fitted using which Gaussians. This clustering problem was tackled using K-means with distance as the proximity measure and the peaks of the modes as the initial

centroid location. The K-means procedure was executed several times and the result of the one with the minimum within-cluster sum of squares was considered.
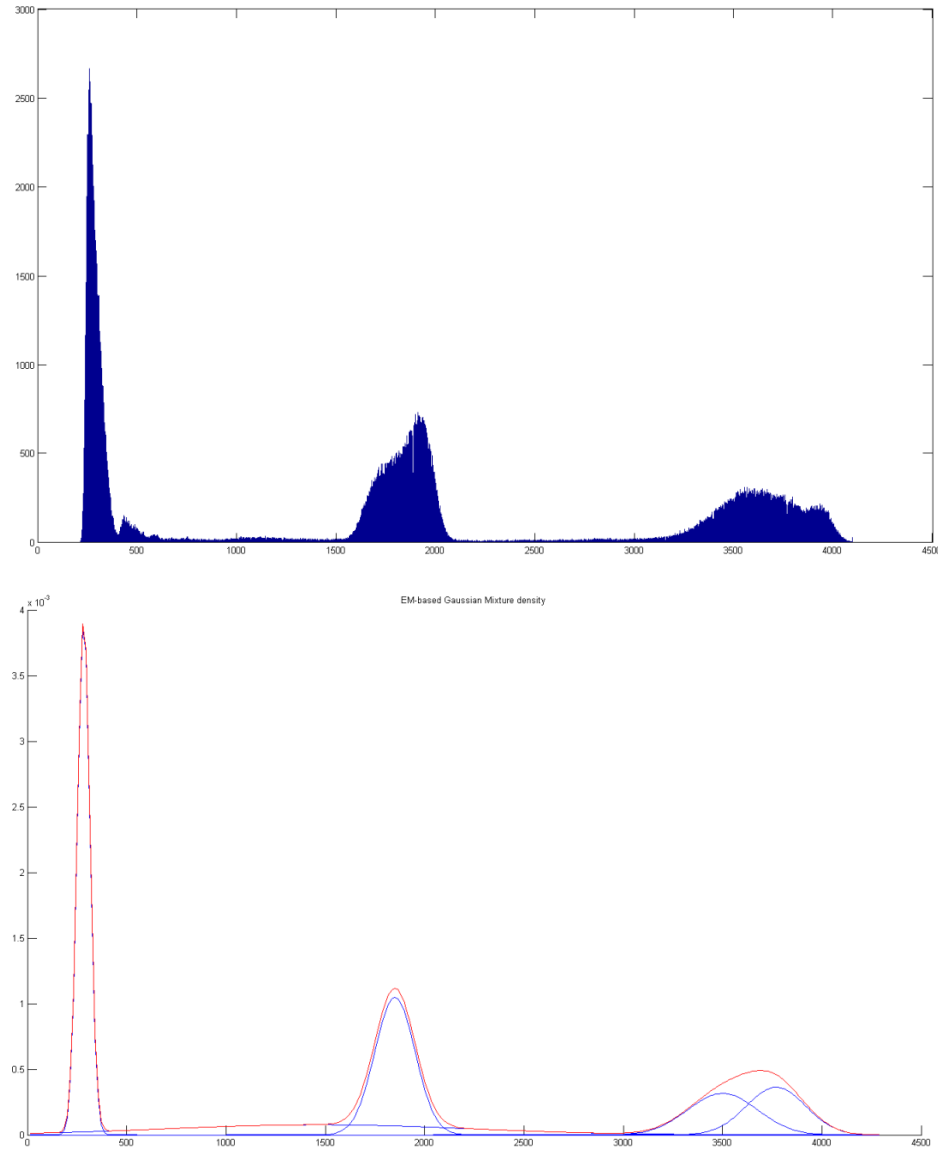
Figure 30. Gaussian mixture model fitted on a histogram

The stretch of the modes i.e. the leftmost and the rightmost extend of the modes was calculated by subtracting and adding, three standard deviations from the mean of the Gaussian if only one Gaussian contributed in fitting the mode. If more

than one Gaussians contributed for fitting a mode, then the leftmost and the rightmost Gaussian's mean and standard deviation were used to determine the spread of the mode.
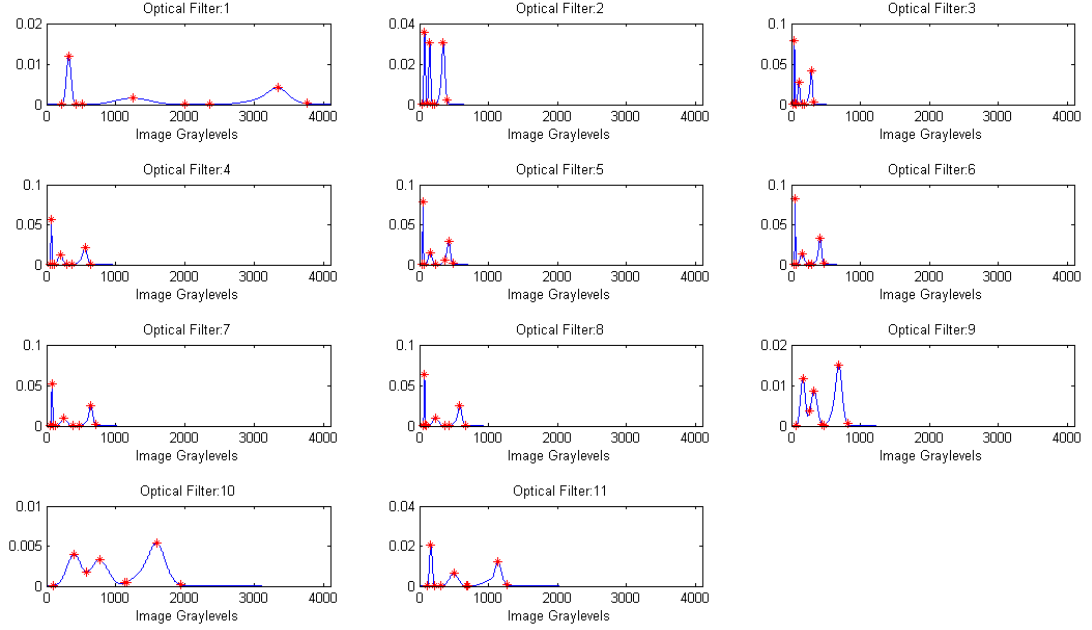
Figure 31. Peaks and the stretch of the modes detected on the normalized curve fitted by gaussian mixture model on the histograms of the gray card images through each optical filter

The piecewise-linear stretching algorithm was just a simple linear stretching carried out between two end points according to the following formula:

$$S = T(r) = \frac{S_{max} - S_{min}}{r_{max} - r_{min}} (r - r_{min}) + S_{min} \qquad \ldots (2)$$

where

$S = $ *Gray level of the output image*

S_{max} *= Rightmost extent of the mode the output image*

S_{min} *= Leftmost extent of the mode the output image*

r *= Gray level of the input image*

43

r_{max} = Rightmost extent of the mode the input image

r_{min} = Leftmost extent of the mode the input image

Figure 31 shows the peaks and the base points detected on the histograms after compensating for the proportion of photons transmitted through the filters.

3.3.   Image registration

The final step in the image processing is image registration. The analysis of the images required tracking the intensity values denoted by gray levels in each of the images captured at different frequency intervals. Therefore, image registration is important to insure that each particular area is analyzed properly in each of the images.

Image registration was implemented using a mutual information based algorithm [18]. The multispectral images have different gray levels for the same scene, due to the use of light from different bands along the spectrum to form the images. In such a case, an intensity based image registration algorithm is not useful as it uses the correspondence in the gray levels between the two images.

The mutual information based algorithm is designed to provide registration for rotational, translational and scaling motion. Little or no dissimilarity is present in the images, but registration of the images is performed to correct minute differences due to motion and scaling due to respiratory movement. The mutual information algorithm uses the joint histogram technique to calculate mutual information between images. The algorithm goes through a series of rotational changes in the clockwise and counter-clockwise directions and translational shift for the additional dimensional change due to image rotation. The images are tested for a scale change, and the combination of rotation, translational shift and scale with highest mutual information is used to correct the image with respect to the reference image. The reference image used is the all pass image, acquired without using an optical filter.

Information theory is based on the amount of information content in a random variable. The information common between two or more random variables is known as mutual information. The amount of information from an outcome of a random variable can be quantified as a logarithm of the inverse of the probability associated with the outcome.

Consider a random variable X, whose entropy H(X) can be expressed as an expectation of the information,

$$H(X) = -\sum p(X = x)log_2(X = x), \qquad \dots (3)$$

where $p(X = x)$ denotes the probability of X at a particular value X = x. Similarly, the joint entropy (2) of random variable X and Y, H(X, Y) is defined as

$$H(X,Y) = -\sum_X \sum_Y p(X = x, Y = y)log_2(X = x, Y = y) \qquad \dots (4)$$

Mutual information I(X, Y) can be defined in terms of entropies calculated as

$$I(X,Y) = H(X) + H(Y) - H(X,Y). \qquad \dots (5)$$

Mutual information between the reference image and the image to be registered is calculated using this method. The combination of rotational and translational shifts with the highest mutual information is used to shift the image to be registered on the reference image.

The three processing steps, the equipment response calibration, the gray card correction and image registration make the raw images acquired from the image acquisition process ready for analysis of the substance imaged, using the properties of spectroscopy.

CHAPTER IV

DATA ANALYSIS

Spectroscopy forms the basis for hyperspectral imaging. The reflectance spectrum obtained from reflectance spectroscopy experiments gives the output in terms of amount of light (number of photons) reflected from the subject of interest. Multispectral and hyperspectral images form from the reflected light. The intensity levels across the from a hyperspectral image cube mimic the reflectance spectra of the material under study.

Spectroscopy uses two techniques, absorption or reflectance. These two techniques are used to study the absorption and reflectance properties of a material or substance as a function of light frequency. The absorption and reflectance properties of a material depend on its chemical composition. Spectroscopy depends on the assumption that chemical composition of every substance is different, which then causes every substance to have different absorption and reflectance properties.

Spectroscopy experiments are conducted by dispersing the transmitted or the reflected light from the sample into its individual components by using a spectrometer. These experiments are carried out under the assumption that the number of photons emitted from the light source are known across the range, so the percentage of absorption and reflectance can be calculated when the detector identifies the number of photons received. In our case, we are concerned with the reflectance properties of the material, because we will capture images using the light reflected from the subject of interest, and the reflectance from the material depends on its light scattering properties.

A spectral signature is a unique reflectance value in a specific part of the spectrum. Every substance, because of its chemical composition, absorbs, transmits

and reflects different amounts of incident electromagnetic radiation. The specific reflectance value obtained at different frequencies is known as spectral signature.

Our subject of interest is reflectance from the surface of the skin, where different layers of the skin have different reflectance properties based on their composition, causing every individual to have a different reflectance response. Many experiments have being conducted to obtain the absorption and the reflectance spectra of skin composition.

The skin is considered the largest organ of the human body. It is divided into two main regions, the epidermis, and the dermis. The epidermis is the most superficial layer of the skin and is constantly regenerated. The dermis is the inner layer of the skin. It supplies the nonvascular epidermis with nutrients through its vascular network [19].

The reflectivity of the skin is a result of the chromophores such as melanin, keratin, carotene, collagen and hemoglobin present in the layers of skin. Keratin is a fibrous protein found in the epidermis that very little effect on the skin reflectance. Carotene, an unsaturated hydrocarbon, and collagen a fibrous protein, are found in the dermis, but they both have little impact of the reflectance spectrum of the skin.

Melanin in the epidermis and hemoglobin in the dermis are the main chromophores in the skin that affect its reflectance properties. Melanin and hemoglobin strongly absorb light in the visible light range and have low absorption in the near-infrared range.

Nishidate, et al., studied the absorption and the reflectance properties on a skin phantom and in-vivo reflectance spectra to estimate the concentrations of melanin and blood oxygen saturation in human skin tissue [20].

The phantom consists of an epidermis and a dermis layer. An agar solution was used as the base material for two of the layers by diluting agar powder in saline by weight in the ratio of 0.8. An intralipid 10% solution by volume was added to the agar solution.

A coffee solution of concentration 5, 10, and 20% by volume was introduced as a substitute for melanin into the 0.1 cm thick base material to be used as epidermis layer. An oxygenated 0.5 cm thick dermis layer was made by adding a small amount of fully oxygenated horse blood having 44% hematocrit. Deoxygenated dermis layer was prepared by dropping a sufficient amount of $Na_2S_2O_4$ rich saline solution on to the surface of the oxygenated dermis layer of the base material. All these layers were hardened by cooling at about 5.5 °C for 30 min. The diffuse reflectance and total transmittance spectra of each layer were measured individually according to the schematic shown in Figure 32.
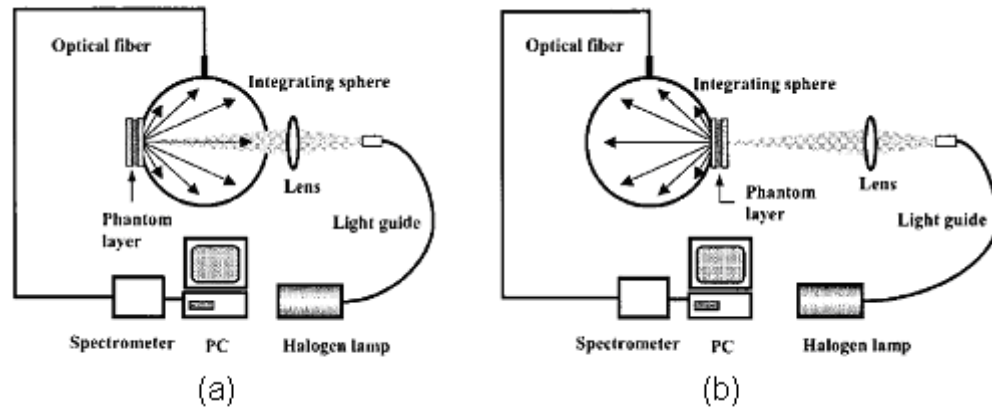

Figure 32. Experimental setups for (a) diffuse reflectance measurements and (b) total transmittance measurements [20]

Steven Jacques at the Oregon Medical Laser Center (OMLC) [21] studied the reflectance spectrum of melanin across the frequency range. Melanin is a complex absorbing material produced by cells called melanocytes. It provides a certain degree

of protection against skin damage from sun exposure, and melanin production increases in response to sun exposure.

Many different types of melanin exist according to the different proportions and bonding patterns of the component molecules. Pheomelanin and eumelanin are the important ones. Pheomelanin is a yellow-to-reddish-brown alkali-soluble material found in red hair. Eumelanin is a black-to-dark-brown insoluble material found in human skin and hair and is the most abundant melanin in humans. The molecular structure of the extended melanin polymer is not unique, and therefore it cannot be well characterized. It is difficult to cite the concentration of melanin in the units of moles/liter. The average epidermal absorption coefficient depends on both the melanosomal (μ_a) and the volume fraction (f_v) of melansomes in the epidermis. Volume fraction is a means of stating mole fraction when dealing with mixtures, when a difference exists between the sizes of the molecules in a mixture. In skin, the volume fraction of melanosomes is estimated to vary with light skinned (f_v = 1-3%), well-tanned (f_v = 11-16%) and darkly pigmented (f_v = 18-43%).

Study of skin reflectance can be explained by the concept of extinction coefficient. In general, extinction coefficient refers to the absorption of light in a medium. It is the imaginary part of the complex index of refraction. The complex index of refraction can be explained from the real and the imaginary part of the index of refraction, where the real part indicates the refractive index (n), while the imaginary part indicates the amount of absorption loss or the extinction coefficient (k) when the electromagnetic wave propagates through the material. Both n and k are dependent, and the higher the extinction coefficient, the more the light is absorbed by the material under study.

The dependence of the extinction coefficients of eumelanin and pheomelanin on wavelength is shown in the figures below, expressed in units of [cm^{-1} (mg/ml)$^{-1}$].
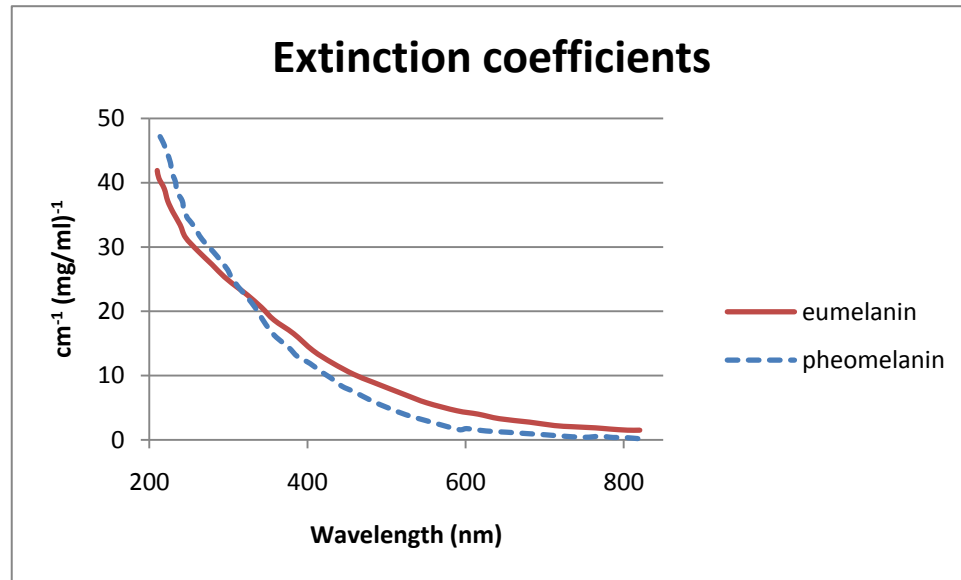
Figure 33. Extinction coefficient of eumelanin and pheomelanin

The hemoglobin spectrum vs. the skin reflectance measurement was studied by Zijlstra, et al., [22], where they observed a unique absorption pattern, the "W" pattern in the 545 nm to 575 nm range. The dermis is the vascular layer of the skin, so it contains hemoglobin in the form of blood. Hemoglobin is a protein contained in the red blood cells that binds very easily to oxygen, which is then transported throughout the body.

The absorption pattern shown in figure 34 occurs only when hemoglobin is bound with oxygen. De-oxygenated hemoglobin exhibits shifted absorption bands, and the distinct 'W' pattern is no longer visible. The majority of hemoglobin in the human blood vessels is oxygenated. Specifically, 90-95% of the Hb in the arteries is oxygenated, while about 45-50% of the Hb in veins is oxygenated.

Scott Prahl from the Oregon Medical Laser Center conducted a study on optical absorption of hemoglobin [23]. His results are shown below in Figure 34.
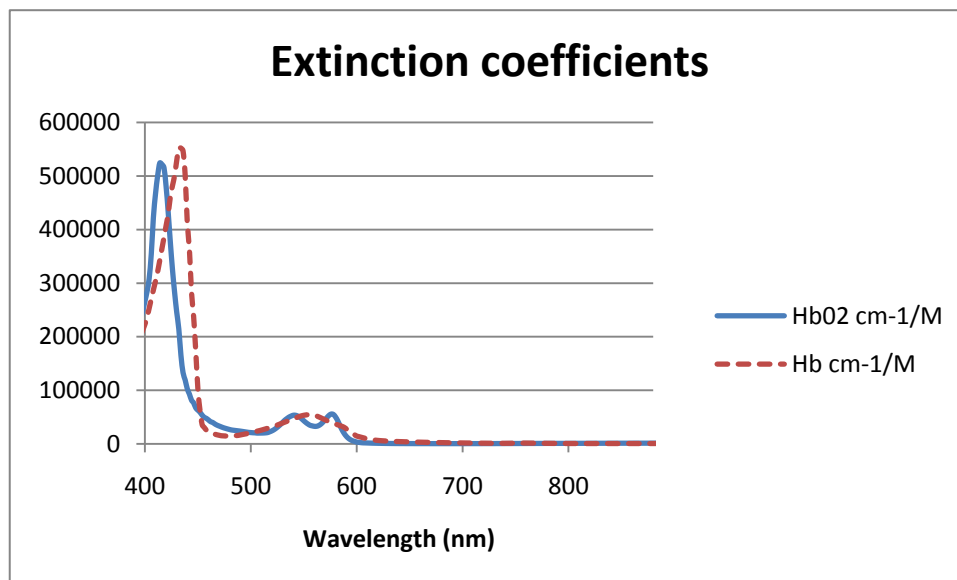
Figure 34. Extinction coefficient of oxy-hemoglobin and deoxy-hemoglobin

One equivalent of hemoglobin is defined as the amount of hemoglobin that contains 1 gm atom of Fe and combines with 1 gm molecule of O_2 or CO. One equivalent of hemoglobin is assumed to be 64,500/4 or 16,125 gm. The values of the hemoglobin (Hb) spectra are typically tabulated in equivalents. A concentration of 10^{-6} equivalent is considered as 16.125 mg of hemoglobin per cc. Therefore, four times as many equivalents are present as hemoglobin molecules.

Absorbance (A_λ) is calculated from the ratio of energy passing through the sample (I_t) to the energy that is incident on the sample (I_i)

$$A_\lambda = -log\left(\frac{I_i}{I_t}\right). \qquad \dots (6)$$

The oxy and deoxy-hemoglobin spectra can also be denoted in terms of molar extinction coefficient. To convert from the molar extinction coefficient (*e*) to absorbance (*A*) for a particular frequency (λ), we multiply the molar extinction coefficient by the molar concentration (C) and the path length (x), according to the Beer-Lambert law.

"Beer-Lambert Law, states that the optical absorbance of a chromophore in a transparent solvent varies linearly with both the sample cell path length and the chromophore concentration" [24].

$$A_\lambda = e_\lambda . x . C \qquad \ldots (7)$$

If *y* is the molar concentration in grams per liter, and normally a 1 cm cuvette is used, then the absorbance is given by

$$A = \frac{2.303 \times e \left[\frac{\frac{1}{cm}}{\frac{moles}{liter}}\right] . y \left[\frac{g}{liter}\right] . 1[cm]}{64500 \, [g/mole]}, \qquad \ldots (8)$$

using 64,500 as the gram molecular weight of hemoglobin. Thus, the apparent absorbance can be shown in Figure 35 below.
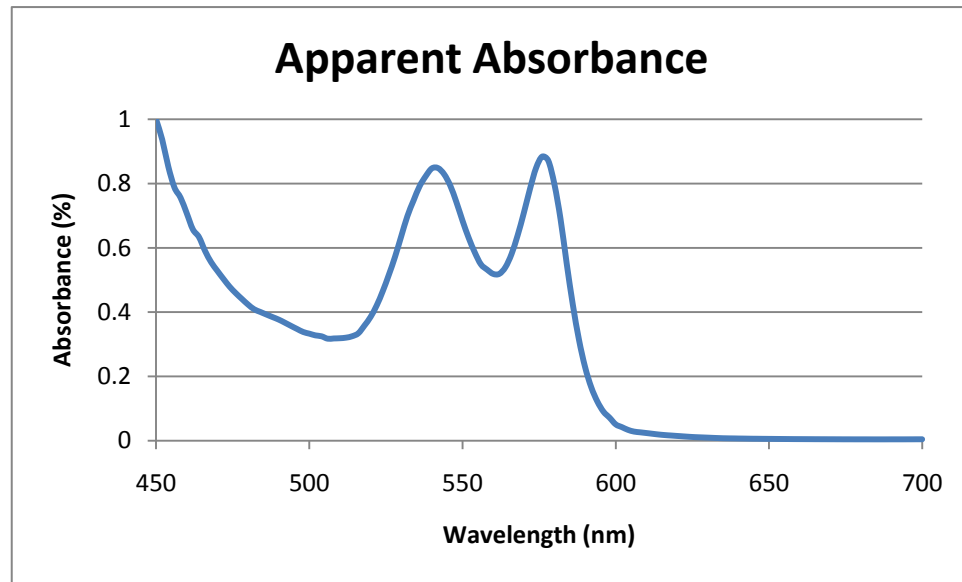

Figure 35. Apparent absorption of oxy-hemoglobin

Karel Zuzak studied the effect on hyperspectral images by controlling the amount of blood flow to the arm using a blood pressure cuff [10]. Hyperspectral images of the normal arm were first taken to form the baseline images for comparison. Images were taken 2 minutes after an occlusion of 140-150 mm Hg was made using

the cuff. The pressure was released and four consecutive reperfusion measurements were taken, with the first immediately after the release of cuff and then the next three readings after intervals of 2 minutes. Nine subjects, 5 men and 4 women, were imaged by this process. The hyperspectral images consisted of 121 images from 525 to 645 nm in 1 nm wide bands. For the reference sample spectra, pure oxy-hemoglobin and deoxy-hemoglobin were prepared by using blood from healthy, non-smoking individuals. These reference spectra are useful to deconvolve the visible spectra for the images into percentages of oxy-hemoglobin and deoxy-hemoglobin, using a multivariate least squares algorithm.

The visible spectra obtained from the images is quantified as the apparent absorbance, a ratio of reflected sample radiation *R*, and the reflected radiation from reference sample *Ro*, measured along the wavelengths for each pixel of the image representing a small area of interest. The absorbance spectrum for each pixel, denoted by x and y, is given by the following equation.

$$A(x, y, \lambda i) = \log\left(\frac{Ro(x, y, \lambda i)}{R(x, y, \lambda i)}\right) \qquad \ldots (9)$$

The apparent absorbance spectrum is considered to be a mixture of oxy-hemoglobin and deoxy-hemoglobin. To transform this spectrum into percentages of pure oxy-hemoglobin and deoxy-hemoglobin, it is deconvolved into the two components. The visible spectrum is deconvolved by performing a least-squares fit for each pixel to determine the best linear combination of the reference spectrum of oxy-hemoglobin and deoxy-hemoglobin. The following equation shows the multivariate regression equation to be calculated for each pixel.

$$C(k, j) = S(k, \lambda i)R(j, \lambda i) + e(k, j) \qquad \ldots (10)$$

where *C* is a linear, deconvolved contribution matrix, k specifies one of the two pure quantities oxy-hemoglobin and deoxy-hemoglobin, and j equals x*y is the total number of pixels. *R* is the matrix of observed spectral values from unknown samples,

and *e* is a matrix of residuals from regression analysis. *S* is the sensitivity matrix given by

$$S(k, \lambda i) = \left(P^t(k, \lambda i)P(k, \lambda i)\right)^{-1}P^t(k, \lambda i), \qquad \dots (11)$$

where *P* is the matrix of pure components obtained from the spectral analysis against the reference sample.

The above procedure can be applied to separate multiple components of a single sample, provided that their individual independent reference components from the particular imager are known.

The objective of this thesis is to build a system to act as a test bed for choosing optical filters to suit a particular experiment such as detection of a particular reference pattern that could be used to determine the substance under study. In this case, the condition of wounds or the health of the skin according to the oxy- and deoxy-hemoglobin content in the superficial layer of the skin is of interest.

Matching the intensity values in the image to the range of the corresponding filter is necessary to form apparent response from the hyperspectral image cube. The response of the system, i.e. the light source, the camera and the optical filters must be corrected to obtain an unbiased response. The effective bandwidth of the filters is considered to be full width half maximum (FWHM) for all the filters. Figure 36 shows the least squares line fitted to the system response within the (FWHM) effective band width.

This least squares fitted line can be used to approximately map the system response within the effective bandwidth to the intensity levels in the image. The lower end corresponds to the darkest gray level in the image, and the higher end corresponds to the brightest gray level.

We compare the fitted line across the effective bandwidth and the range of gray levels in the image. To match the gray levels with the reference spectra we divide the frequency range into a certain number of bins. The range of gray levels in the image is also divided into the same number of bins.
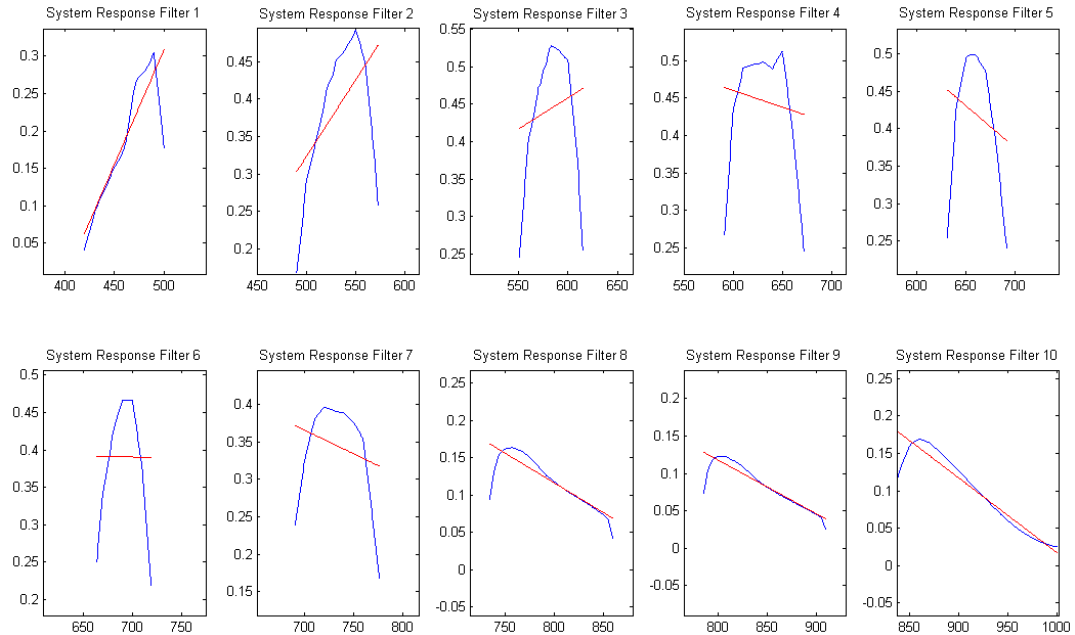

Figure 36. Response of system for each filter within (FWHM) effective bandwidth with their OLS fit
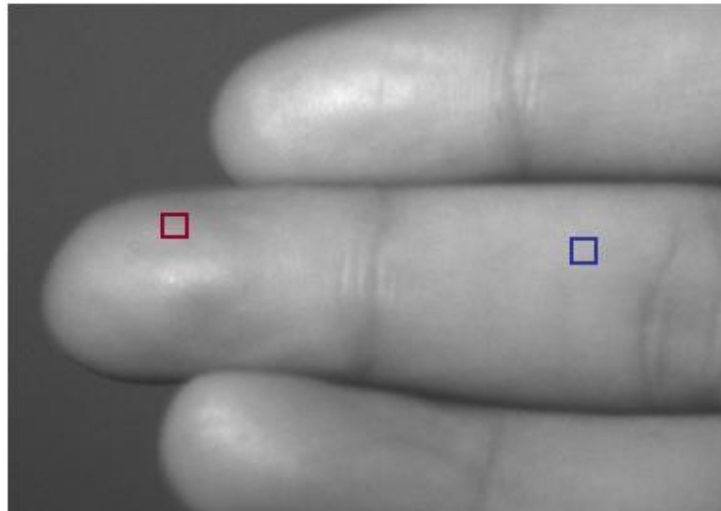

Figure 37. Image of the finger showing more blood flow near the tip

For example, if the bandwidth of a filter is 60 nm and the dynamic range of the gray levels of the image acquired from the filter is 600. The bandwidth and the grayscale range are divided into equal number of parts to be plotted against each other.

Figure 37 shows an all pass image with different levels of blood on the surface of the skin (palm with no interference of melanin), and the response within the colored boxes is shown.
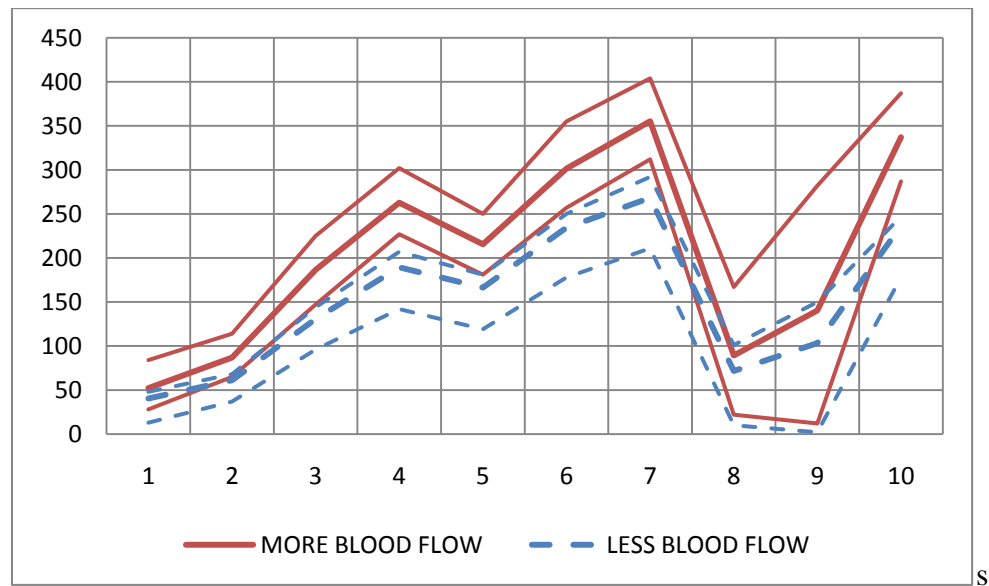
Figure 38. The min, mean and max of the intensity spectra from within the boxes.

It can be seen in the above intensity spectra that the region with more blood flow has a darker shade of gray and with comparatively less blood flow the regions are on the brighter side.

These spectra can be matched with the reference spectra of oxy-Hemoglobin and deoxy-Hemoglobin. Similarity of this intensity value pattern to the reference pattern denotes the presence of the reference materials, and the shift in the pattern denotes the concentration of oxy-Hemoglobin in the skin region of the subject.

Note that the 'W' pattern in the hemoglobin response is not prominent, but a somewhat similar trend is visible. This proves that the current sets of filters are ineffective in accurately detecting the pattern of oxy-hemoglobin response.

This experiment proves the point that the apparatus implemented will work as a test bed for making filter choices. Rather than using filters that cover the entire visible light range, filters with bandwidth around 10 nm should be used spread across the range from 500 nm to 600 nm. These filters will capture the 'W' pattern of the oxy-hemoglobin response efficiently and facilitate detection of oxy-hemoglobin in the blood.

Certain factors that must be considered for best results while using this apparatus for hyperspectral or multispectral imaging are stated below.

i.   Use of two cameras instead of one

The camera response is very low in the near infra-red region. Thus calibration becomes mandatory for images taken in this region. Most cameras that work in the visible range tend to have low response in the near infra-red region. A solution for the low camera response in the infra-red region is to use of two cameras. One camera covers the visible region and the other covers the near infrared region, which will make the response across the range similar.

ii.   Flat light response

The system response is calculated using the camera characteristics and the light source characteristics, so a flat light source is beneficial.

iii.   In-band transmittance of the optical filters

The transmittance of filters chosen should be approximately equal. If the peak transmittance and the area under the transmittance curve of the filters are approximately equal then the correction made to the images using calibration and the compensation factor will be minimal.

Correction is applied to the images to make the image intensities independent of the filter response. A flat camera and light response and an approximately equal filter response in terms of area under the response curve and transmittance will lead to image intensities independent of the filter response, reducing the correction effects.

iv.   Linearity of the System

The flat response of the components also provides linearity to the system, which is required for the multivariate regression analysis to find the percentage transmittance of the reference material from the intensity spectra obtained from the images.

v.   Filter selection

Finally, the most important criteria are of the filter selection according to the spectra response of the material under study. The case regarding oxy-hemoglobin detection from the surface of the skin or blood must have optical filters that efficiently pick up the 'W' pattern in the visible range exhibited by oxygenated blood. Therefore, filter selection (i.e. the central frequency and width of passband of the optical filters) must be carefully selected accordingly for each experiment. This can be done effectively by using the implemented test structure, on which the filters can be replaced easily to test filter sets in detecting the material under study.

In conclusion, the mechanical assembly designed in this thesis can be used for capturing multispectral and hyperspectral images and adhering to the above mentioned factors while using the apparatus will lead to best results. This assembly also serves as a prototype which can be further modified for more efficient apparatus for capturing spectral images.

BIBLIOGRAPHY

1. Gonzalez, Rafael C., Woods, Richard, 2nd Edition. *Digital image processing.* 2nd Edition. s.l. : Prentice Hall, 2002. Chapter 6, Color Image Processing. ISBN 0201180758.

2. Vagni, Fabrizio. *Survey of Hyperspectral and Multispectral Imaging Technologies.* s.l. : NATO Research and Technology Organisation, May 2007. p. 44. RTO-TR-SET-065-P3 AC/323(SET-065)TP/44 . ISBN 978-92-837-0071-5.

3. Shippert, Peg. *Why Use Hyperspectral Imagery?* s.l. : American Society for Photogrammetry & Remote Sensing (ASPRS), April 2004.

4. *Introduction to Hyperspectral Image Analysis.* Shippert, Peg. s.l. : Online Journal of Space Communication, 2003.

5. Palmer, Christopher. *Diffraction Grating Handbook, 5th Edition.* [ed.] Erwin Loewen. s.l. : NY Thermo RGL 2002. ISBN B000XLMD60.

6. Nicholas M. Short, Sr. *rst.gsfc.nasa.gov.* [Online] http://rst.gsfc.nasa.gov/Intro/Part2_5a.html.

7. *www.hyspex.no.* [Online] Norsk Elektro Optikk A/S. http://www.hyspex.no/index.htm.

8. *A CCD Camera-based hyperspectral imaging system for stationary and airborne applications.* C. Yang, J. H. Everitt, M. R. Davis, and C. Mao. 2, s.l. : GeocartoInternational, 2003, Vol. 18, pp. 71-80.

9. Suresh, Swetha. *Visible to near infrared hyperspectral imaging: visualizing the neurological and biochemical nature of ischemic tissue.* Arlington : s.n., December 2008.

10. *Visible Reflectance Hyperspectral Imaging: Characterization of a Noninvasive, in Vivo System for Determining Tissue Perfusion.* Karel J. Zuzak, Michael D. Schaeberle, E. Neil Lewis, and Ira W. Levin. 9, s.l. : Analytical Chemistry, May 2002, Vol. 74, pp. 2021–2028. DOI: 10.1021/ac011275f.

11. *Imaging Spectroscopy Using Tunable Filters: A Review.* Gata, Nahum. s.l. : Proc. SPIE, 04/2000, Vol. 4056, pp. 50-64.

12. *Novel Hyperspectral Imager Aids Surgeons.* Karel Zuzak, Robert Francis, Jack Smith, Chad Tracy, Jeffrey Cadeddu, and Edward Livingston. s.l. : Biomedical Optics & Medical Imaging, December 2008. DOI: 10.1117/2.1200812.1394.

13. Square Filter Holder For Imaging Lenses - Edmund Optics. *www.edmundoptics.com.* [Online] Edmund Optics Inc. http://www.edmundoptics.com/images/catalog/2839b.jpg.

14. User Guide Universal Motion Interface (UMI)-7764. [Online] ftp://ftp.ni.com/support/manuals/370943a.pdf.

15. Baker, Christopher. 1394 Camera Driver - Main. *www.cs.cmu.edu.* [Online] http://www.cs.cmu.edu/~iwan/1394/.

16. Allied Vision Technologies. Guppy F146B datasheet.

17. Owner's Manual Model 2900 Tungsten Halogen Light Source. *www.illuminationtech.com.* [Online] Illumination Technologies Inc.

18. *Image registration methods: a survey.* Barbara Zitova, Jan Flusser. s.l. : Image and Vision Computing, 2003, Vol. 21, pp. 977–1000.

19. Angelopoulou, Elli. *The Reflectance Spectrum of Human Skin.* s.l. : University of Pennsylvania Department of Computer and Information Science , December 1999. MS-CIS-99-29.

20. *Estimation of melanin and hemoglobin in skin tissue using multiple regression analysis aided by Monte Carlo simulation.* Izumi Nishidate, Yoshihisa Aizu and Hiromichi Mishina. 4, s.l. : Journal of Biomedical Optics, 2004, Vol. 9, pp. 700–710.

21. Jacques, Steven. Optical Absorption of Melanin. *omlc.ogi.edu.* [Online] Oregon Medical Laser Center. http://omlc.ogi.edu/spectra/melanin/index.html.

22. *Absorption Spectra of Human Fetal and Adult Oxyhemoglobin, De-Oxyhemoglobin, Carboxyhemoglobin, and Methemoglobin.* W. G. Zijistra, A. Buursma, and W. P. Meeuwsen-van der Roest. 9, s.l. : Clinical Chemistry, 1991, Vol. 37.

23. Prahl, Scott. Optical Absorption of Hemoglobin . *omlc.ogi.edu.* [Online] Oregon Medical Laser Center . http://omlc.ogi.edu/spectra/hemoglobin/index.html.

24. Beer-Lambert Law. *www.oceanoptics.com.* [Online] Ocean Optics, Inc. http://www.oceanoptics.com/technical/beerslaw.asp.